RIGA TECHNICAL UNIVERSITY

Ance Pļavniece

LIGNOCELLULOSE BASED NANOPOROUS CARBON MATERIALS FOR FUEL CELLS

Summary of the Doctoral Thesis

RTU Press
Riga 2021

RIGA TECHNICAL UNIVERSITY

Faculty of Materials Science and Applied Chemistry
Institute of General Chemical Engineering

Ance Pļavniece
Doctoral Student of the Study Programme "Chemical Technology"

LIGNOCELLULOSE BASED NANOPOROUS CARBON MATERIALS FOR FUEL CELLS

Summary of the Doctoral Thesis

Scientific supervisors
Dr. sc. ing.
AIVARS ŽŪRIŅŠ
Professor Dr. sc. ing.
JĀNIS LOČS

Scientific advisor
Dr. habil. chem. GALINA DOBELE

RTU Press
Riga 2021

Pļavniece A. Lignocellulisic Nanopouros Carbon Materials for Fuel Cells. Summary of the Doctoral Thesis. – Riga: RTU Press, 2021. – 40 p.

Published in accordance with the decision of Promotion Council "RTU P-01" of 22 June 2021, Minutes No. 04030-9.1/24.

The Doctoral Thesis has been developed in the Latvian State Institute of Wood Chemistry between 2012 and 2020 within the framework of the following research programmes:

1. National Research Programme "Exploration, Sustainable Use of Forest and Subsoil Resources – New Products and Technologies" (ResProd) Project 3 "Biomaterials and Bioproducts from Forest Resources with Multiple Uses", 2015–2018.
1. European Research Area Network "Wood-based Carbon Catalysts for Low-temperature Fuel Cells (WoBaCat)", 2016–2019.
2. Fundamental and applied research "Nanostructured Nitrogenated Carbon Materials as Promoters in Energy Harvesting and Storage Technologies (NN-CARMA)", 2018–2021.

https://doi.org/10.7250/9789934226830
ISBN 978-9934-22-683-0 (pdf)

DOCTORAL THESIS PROPOSED TO RIGA TECHNICAL UNIVERSITY FOR THE PROMOTION TO THE SCIENTIFIC DEGREE OF DOCTOR OF SCIENCE

To be granted the scientific degree of Doctor of Science, the present Doctoral Thesis has been submitted for the defence at the open meeting of RTU Promotion Council on November 11 2021 at 14:00 at the Faculty of Materials Science and Applied Chemistry of Riga Technical University, 3/7 Paula Valdena Street, Room 272 and at the following link: https://rtucloud1.zoom.us/j/9352086644.

OFFICIAL REVIEWERS

Professor Dr. sc. ing. Sergejs Gaidukovs,
Riga Technical University

Dr. sc. ing. Vladimirs Biziks
Georg-August-Universität Göttingen, Germany

Dr. habil. chem. Yuriy A. Maletin
Institute for Sorption and Problems of Endoecology, Ukraine

DECLARATION OF ACADEMIC INTEGRITY

I hereby declare that the Doctoral Thesis submitted for the review to Riga Technical University for the promotion to the scientific degree of Doctor of Science is my own. I confirm that this Doctoral Thesis had not been submitted to any other university for the promotion to a scientific degree.

Ance Pļavniece ……. (signature)
Date: ……

The Doctoral Thesis has been written in Latvian. It consists of Introduction; 4 chapters; Conclusions; 41 figures; 20 tables; the total number of pages is 92, not including appendices. The Bibliography contains 183 titles.

ACKNOWLEDGMENTS

I express sincere gratitude to my scientific supervisors – Lead Researcher Dr. sc. ing. Aivars Žūriņš and Professor Dr. sc. ing. Jānis Ločs, for their supervision, timely assistance, patience and moral support throughout the development of the Thesis.

I express sincere gratidue to my scientific advisor – Lead Researcher Dr. habil. chem. Gaļina Dobele for advice, assistance, understanding and support regarding any questions related to the Thesis.

I am grateful to the Director of the Latvian State Institute of Wood Chemistry Dr. sc. ing. Uģis Cābulis for providing infrastructure during the development of the Thesis in the Biorefinery laboratory.

Thank you to my colleagues in Latvian State Institute of Wood Chemistry, especially leading researcher Dr. sc. ing. Jānis Rižikovs, researcher Dr. sc. ing. Aleksandrs Voļperts, leading researcher Dr. sc. ing. Aigars Pāže and researcher Dr. chem. Kristīne Meile for their advice and moral support; scientific assistant Mg sc. Ralfs Pomilovskis, scientific assistant Mg. chem. Velta Fridrihsone, scientific assistant Mg sc. Lilija Jašina, researcher Dr. chem. Anrijs Verovkins, scientific assistant Mg. chem. Vilhelmīne Jurkjāne, scientific assistant Dmitrijs Djačkovs, Dr. chem. Dzintra Vilsone, and my colleagues in Riga Technical University for performing analysis, for assistance and useful advice throughout the experimental work.

Thank you to leading researcher Dr. phys. Ivar Kruusenberg and researcher Mg. sc. Kätlin Kaare (National Institute of Chemical Physics and Biophysics, Tallin, Estonia) for cooperation and asisstance in testing catalysts for oxygen reduction reaction.

Thank you to leading researcher Dr. phys. Jānis Kleperis and scientific assistant Ingars Lukoševičs (Institute of Solid State Physics, University of Latvia) for cooperation and assistance with XPS spectrometry.

Thank you to leading researcher Dr. Loreta Tamasauskaite-Tamasiunaite, Professor Dr. habil. Eugenijus Norkus (Center for Physical Sciences and Technology, Vilnius, Lithuania) for cooperation and assistance with Raman spectrometry, SEM and TEM.

And my most heartfelt gratitude to my family for their understanding, support and patience!

TABLE OF CONTENTS

LIST OF ABBREVIATIONS

ABL – activated carbon on bio-oil base;
AC – activated carbon on cellulose base;
AHTK – activated carbon after HTK;
AMA – activated carbon on black liquor base;
AO – activated carbon;
ASD – activated carbon on pulp mill sewage sludge base;
AWC – activated carbon on wood char base;
BET – Brunauers-Emets-Tellers (method);
DCDA – dicyandiamide;
DMF – dimethylformamide;
DR – Dubinin-Radushkevich (equation);
HTK – hydrothermal carbonisation;
IUPAC – International Union of Pure and Applied Chemistry;
K = 1;2;3 – raw material to activator mass ratio 1: 1; 1: 2; 1: 3;
LG – levoglucosan;
MEL – melamine;
N-dopēšana – doping with nitrogen;
OM – carbon materials;
ORR – oxygen reduction reactions;
PirK – pyrolyzed wood;
SEM – scanning electron microscopy;
T_{akt} – activation temperature;
WC – wood char (SIA "Fille 2000", Latvia);
XPS – X-ray photoelectron spectroscopy.

INTRODUCTION

The use of renewable energy sources (solar, wind and water) in electricity generation is still not enough to meet humanity's growing energy demand. That is why the documents of the World Economic and Energy Forums emphasize the importance and need for the use of renewable energy sources such as fuel cells. Mobile, renewable energy sources are essential for both portable electronics (mobile phones, laptops, tablets, etc.) and vehicles. Research and development of fuel cell technologies, as well as the improvement of their properties, are widely studied all over the world. The main problem is the high price of fuel cells where the main source of costs is the platinum required in the catalyst. In 2014, the EU established a list of critical raw materials (CRMs) which are economically and strategically important but with high supply risk and which included 54 precursors of which platinum was included in the high-risk group [1].

Technologies that use biomass as a raw material for the production, transformation and storage of electrical energy are attracting scientific interest worldwide. The main reasons for this are current research into new energy sources and the environmental problems caused, for example, by the release of greenhouse gases during the combustion of fossil fuels to generate electricity.

Activated carbon (AO) is a multifunctional material that due to its sorption, ion exchange, complex formation, electrochemical and catalytic properties can be used in a wide range of applications. AO materials have a large surface area, electrical conductivity and heat resistance. It is also known that microporous AO materials can be synthesized from lignocellulose precursors by chemical activation. As a result, AO is inexpensive, has a highly developed specific surface area, and can be used as high-quality sorbent and catalyst. Alkali metal compounds are most often used as activators for the synthesis of such materials. Another advantage of AO materials is the ability to modify them, which expands their scope. The introduction of various heteroatoms into the structure of activated carbon makes them more active in electron transfer processes, such as the reduction of molecular oxygen and electropositive metals, the oxidation of volatile hydrides and organic compounds.

Among the various heteroatoms (N, B, P, S) used in practice, nitrogen is the most advantageous for modifying carbon materials because the sizes of N and C atoms are similar, as well as because a strong covalent bond is formed between them. Theoretical studies have shown that nitrogen can be considered as an n-type donor that transfers electrons to carbon. Doped AO, as a catalyst for the reduction of oxygen in fuel cells to convert chemical energy into electricity, is not only a promising new application of carbonaceous materials, but can also contribute to solving energy storage and conversion problems.

Despite many efforts by researchers to improve the productivity, efficiency and durability of fuel cell technology, the large-scale commercial use of metals, especially platinum group-free catalysts, is problematic. Therefore, the task is still to develop a cheap, platinum-free catalyst for fuel cells with similar or higher electrochemical activity and stability.

Aim and tasks of the Doctoral Thesis

The aim of the dissertation is to obtain nitrogen-doped, biomass-derived carbon materials of various structures by chemical activation, which could be used in fuel cells.

To achieve the aim, the following tasks have been set:

1. Obtain carbon materials with a developed surface area and a certain porosity by using various raw materials (wood, pulp, pulp mill waste products (pulp mill effluent sludge, black liquor), birchwood bio-oil) with different carbonisation methods (thermal and hydrothermal) and subsequent activation.
2. Obtain modified carbon materials by doping them with nitrogen.
3. Determine and compare the porous structure, nitrogen content and electrochemical properties of the obtained doped carbon materials depending on the precursors and extraction conditions.

Scientific significance and novelty

Systematic research has been carried out and new findings have been obtained on the lignocellulosic biomass carbonisation, thermochemical activation and nitrogen doping process parameters influence on the specific surface area and pore volume of the obtained doped activated carbon. It has been shown that the use of hydrothermal carbonisation can increase the yield of porous activated carbon and improve its electrochemical activity.

For the first time, nitrogen-doped activated carbon was obtained on the basis of lignocellulose biomass with an adjustable micro- and mesoporous structure, regularities between the parameters of the porous structure and their electrochemical properties were determined. Nitrogen-doped activated carbon catalysts based on lignocellulose biomass have been obtained, which are able to provide equivalent and higher activity in fuel cells as a commercial Pt / C catalyst.

Practical significance

Studies have shown that high-efficiency micro- and mesoporous activated carbon with high added value can be obtained on the basis of lignocellulose biomass in a three-stage thermochemical process.

A methodology has been developed for the synthesis of nitrogen-doped activated carbon by synthesis with dicyandiamide in dimethylformamide suspension as a raw material using wood, its processing residues and wood char.

Based on the experimental data, a production technology has been developed, requirements for technological equipment have been determined, material and heat balances of processes for obtaining nitrogen-doped activated carbon from Latvian natural resources have been compiled. The developed methodology and material balance can be used as input data for the design of a nitrogen-doped activated carbon plant in Latvia.

Thesis statements to be defended

1. The porosity of activated carbon depends on the activation conditions and the properties of the raw materials.

2. The environment of the carbonisation process affects the further porous structure of the material after activation and doping.

3. There is a relationship between the pore size distribution in the carbon material structure and the ability of the catalyst to reduce oxygen to its surface.

Approbation of the reserch results

The main results of the Thesis have been summed up and presented in 10 international scientific conferences and published in 7 scientific publications.

Publications:

1. **A. Pļavniece**, A. Zhurinsh, G. Dobele, A. Volperts. Impact of biomass derived raw material on nitrogen doped porous carbon structure. *Key Engineering Materials, 762, (*2018*), 99–103.*(Scopus)
2. **A. Pļavniece**, G. Dobele, A. Volperts, A. Zhurinsh. Wood-based nitrogen doped activated carbon for fuel cells. *IOP Conf. Ser.: Mater. Sci. and Eng.* 503, (2019), 012011. (Scopus)
3. **A. Pļavniece**, A. Zhurinsh, G. Dobele, J. Locs. Chemical activated hydrochar flakes from birch wood. *Key Engineering Materials* 800, (2019), 261–266. (Scopus)
4. A. Volperts, **A. Pļavniece**, G. Dobele, A. Zhurinsh, I. Kruusenberg, K. Kaare, J. Locs, L. Tamasauskaite-Tamasiunaite, E. Norkus. Biomass based activated carbons for fuel cells and supercapacitors. *Renewable Energy,*141, (2019), 40–45. (Scopus)
5. **A. Pļavniece**, G. Dobele, A. Volperts, A. Zhurinsh, K. Kaare, I. Kruusenberg, J. Locs. Chemically activated and N-doped hydrochar flakes as a fuel cell catalysts. Proceedings of short papers “Alternative energy sources, materials and technologies (AESMT’20)” Publishing House: “Imeon” Sole-owner, 2, (2020), 79–80. ISSN 2603-364X
6. **A. Pļavniece**, G. Dobele, A. Volperts, A. Zhurinsh, K. Kaare, I.Kruusenberg, J. Locs. "Chemically Activated N-doped Hydrochar flakes and Char for energy applications" *Special Issue C "Bulgarian Chemical Communications"*, 52, (2020), 20–25. (Scopus)
7. **A. Pļavniece**, A. Volperts, G. Dobele, A. Zhurinsh, K. Kaare, I. Kruusenberg, K. Kaprans, A. Knoks, J. Kleperis. Wood and Black Liquor-Based N-Doped Activated Carbon for Energy Application. *Sustainabillity*, 13, (2021), 9237. (Scopus).
8.

Presentations in conferences

1. Riga Technical University 58th International Scientific Conference "Materials Science and Applied Chemistry" 2017, 20.10.2017, Riga , Latvia, (oral report).
2. 34th Scientific Conference of the Institute of Solid State Physics (within the framework of the 76th Scientific Conference of the University of Latvia), 20–22.02.2018, Riga, Latvia, (poster report).
3. Alternative energy sources, materials and technologies. AESMT’18, 14–15.05.2018, Plovdiv, Bulgaria, (poster report).
4. Functional materials and nano tehnologies, FMNT 2018, 3–5.10.2018, Riga, Latvia (poster report).

5. Riga Technical University 59th International Scientific Conference "Materials Science and Applied Chemistry" 2018, 26.10.2018, Riga, Latvia, (poster report).

6. Alternative energy sources, materials and technologies. AESMT'19, 3–4.06.2019 , Sofia, Bulgaria, (poster report).

7. Alternative energy sources, materials and technologies. AESMT'20, 8–9.06.2020, Varna, Bulgaria, (poster report), (online).

8. Riga Technical University 58th International Scientific Conference "Materials Science and Applied Chemistry", MSAC 2020, 23.10.2020, (oral report), (online).

9. 37th Scientific Conference of the Institute of Solid State Physics (within the framework of the 79th Scientific Conference of the University of Latvia), 23–25.02.2021, Riga, Latvia, (oral report), (online).

10. Green Carbon 2020, International Symposium on Functional Biomass-derived Carbon Materials, 9–11.03.2021, Saragos, Spain, (poster report), (online).

1. SUMMARY OF LITERATURE REVIEW

The literature review summarises the literature on the methods of obtaining and analysis of nitrogen-doped activated carbon materials, their structure and properties, as well as the structure and operating principles of fuel cells.

Activated carbon (AO) is a multifunctional material that can be used in a wide range of applications due to sorption, ion exchange, complex formation, electrochemical and catalytic properties. Biomass is a widespread renewable resource both in Latvia and around the world. Biomass-based activated carbon is relatively inexpensive, has a highly developed specific surface area and can be used as a high-quality sorbent and catalyst. The cost of carbon nanotubes or graphene far exceeds the price of AO, especially for the most efficient single-layer nanotubes.

One of the most important properties of carbon materials (OM) is the pore structure, which determines the surface area and mass transfer to chemical and ionic groups. OMs with pore sizes below 100 nm are called nanoporous, but according to IUPAC, pores are classified according to their size [2]. The pores are divided into three groups: micropores (diameter < 2 nm), mesopores (diameter 2–50 nm) and macropores (diameter > 50 nm) [2]. In typical carbon materials, a large number of micropores provides a large surface area due to the high surface area to volume ratio. Mesopores, on the other hand, provide more efficient mass transfer than micropores. However, most materials have both mesopores and micropores, which balance these two effects by providing a large surface area and efficient mass transfer. Thus, the pore distribution is very important because it determines the performance of the material. Elemental microstructural carbonate fragments obtained in the first stage of the synthesis of nitrogen-doped activated carbon form a carbon scaffold with a certain functional composition and structure, which plays an important role in the formation of nanopores during further thermochemical activation. Changes in texture parameters during carbonisation allow the production of activated carbon with controlled porous surface parameters, nanopore volume and pore size distribution to ensure easy access to electrolytes.

The choice of raw material and the carbonisation conditions have a very large influence on the porous structure and properties of the obtained carbon material. The parameters of carbonisation and activation change not only the texture of the material, but also the degree of graphitisation and the functional groups, and as a result of the complex interaction of these three factors, the conductivity of the material also changes. However, there are no data in the literature on the optimal parameters of the porous structure of activated carbon, the desired types of raw materials and the application of different heat treatment methods.

The development of materials for electricity generation, transformation and storage using biomass carbon materials as precursors is of scientific importance worldwide due to the properties of activated carbon such as high electrical and thermal conductivity as well as good chemical and thermal stability in both acidic and basic environments. Due to these properties, it is the most widely used material in electrochemical devices such as batteries, capacitors and low temperature fuel cell cells. In low temperature fuel cells, carbon materials are used as

structural components in polymer membranes of bipolar plates and gas diffusion layers, as well as in electrodes as catalyst substrate materials.

Recently, N-doped carbon has attracted a lot of attention because some of its properties surpass platinum. N-doped carbon materials have been shown to have sufficiently promising properties to be used as catalysts in low-temperature fuel cells, which are electrochemical devices that convert chemical energy into electrical energy. At present, it is not clear whether electrocatalytic performance is directly related to the total nitrogen content, or whether it is not its quantity but the location and type of nitrogen binding in the porous carbon matrix that matters. Nitrogen atoms in pyridine or graphitic nitrogen-containing groups are considered to be the major centres of oxygen reduction reaction activity, and N-doping enhances the catalytic activity of carbon itself. Although researchers use different nitrogen precursors, change the raw materials and the reaction environment, the optimal conditions for the synthesis of N-doped carbon materials have not yet been found.

2. EXPERIMENTAL SECTION

The experimental course of the dissertation, the methods of analysis used and the results to be obtained, the main processes and the changes in the structure of the material taking place in them are schematically shown in Fig. 1.

Six types of lignocellulosic biomass raw materials with different carbon content and low nitrogen content were used in the study: birch wood, wood char (SIA "Fille 2000", Latvia), cellulose, black liquor (lignin-containing by-product of cellulose production), pulp mill effluent (CRN) sludge (Horizon Pulp and Paper Ltd.) and bio-oil (obtained at the Latvian State Institute of Wood Chemistry in a rapid pyrolysis plant after the release of levoglucosan (LG)). 3-stage heat treatment synthesis was used to obtain N-doped AO. In the first stage of the synthesis, the material was carbonised by two different methods:

1. The raw material was heated in a kiln (heating rate 3 ° / min) to a temperature of 400 °C to 500 °C under a stream of argon and kept at this temperature for 2 to 6 hours.
2. The raw material (300 g of absolutely dry birch chips) and water (4000 g) are placed in a stainless-steel autoclave where it is heated from 180 °C to 250 °C and kept at this temperature for 1, 2, 4, 6, 12 hours and then cooled to room temperature. The carbonate is separated from the aqueous solution by filtration and then dried in a drying oven at 105 ± 2 °C.

The second stage is thermochemical activation. The carbonised material is ground in a Pulverisette 5 (*Fritsch*) ball mill to obtain a material with an even distribution of particles. The prepared material (50 g) in a polypropylene container was mixed with a dry activator (NaOH) having a weight ratio to the absolutely dry starting mass of K (K = 1 – 4), then H_2O (80 ml) is added and shaken vigorously for 5 min. The obtained mass was transferred to a stainless-steel container with a lid. Activation was performed for 60 minutes at 600–800 °C under an argon flow (200 l / h) using a *Nabertherm L40/11* kiln manufactured in Germany, in which the temperature was controlled with *Controltherm MV* software. After activation, the AO pores were filled with residual unreacted activation reagent and the resulting sodium salts. In order to get a quality product, it is necessary to clean the AO. This is done through a demineralisation process. Previous studies have shown [3] that higher quality AO can be obtained in a demineralisation process using HCl. Based on the obtained results, demineralisation of 2 hours of AO with 10 % HCl and rinsing with demineralised water to pH 5–6 was used in this work. The demineralised material was dried for 12 hours in a drying oven at 105 ± 2 °C.

The third stage is doping, which was done with two reagents:

1. In a glass round flask, the obtained AO powder was mixed with dicyandiamide (1:20 by weight), DMF was added and mixed to give a black suspension. The round flask is placed in a rotary evaporator. The resulting material is then heated in a Nabertherm kiln (heating rate 4 °/ min) to 800 °C and maintained at this temperature for 2 hours.
2. The obtained AO powder was mixed with melamine (1:1 by weight) and placed in a *Pulverisette 5* ball mill where it was homogenised for 1 hour (speed 300 rpm). The resulting material was then heated in a *Nabertherm* kiln (heating rate 4 °/ min) to 800 °C or 950 °C and maintained at these temperatures for 2 hours.

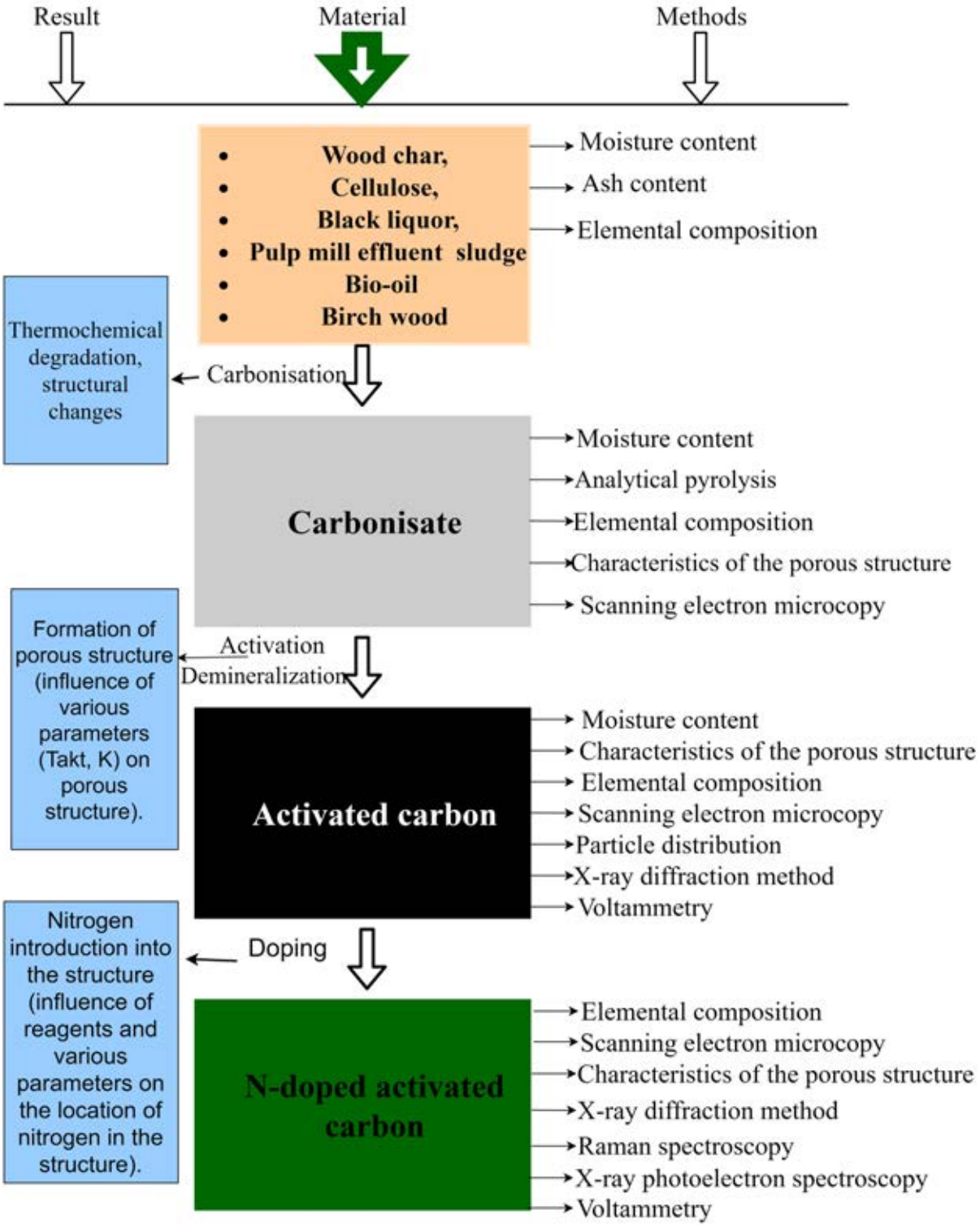

Fig. 1. Analytical methods used.

To study the ORR kinetics, linear scanning voltammetry curves were recorded using rotating disk electrodes (RDE). Then, using the *Koutecký-Levich* model, the linear scanning voltammetry curves are processed [4], [5] according to the equation:

$$\frac{1}{j} = \frac{1}{j_k} + \frac{1}{j_d} = \frac{1}{j_k} + \frac{1}{0{,}62nFD_{O_2}^{2/3}v^{-1/6}C_{O_2}^{b}\omega^{1/2}} \ , \quad (1.1)$$

where

j – total current density, A;

j_k – kinetic current density A;

j_d – diffusion limited current density, A;

F – Faraday constant (96 486.4 C·mol^{-1}), C·mol^{-1};

ω – electrode rotation speed, rad·s^{-1};

C_{O2} – O_2 concentration in the electrolyte, mol·cm^{-3};

D_{O2} – diffusion coefficient;

v – kinematic viscosity of the electrolyte, cm^2 · s^{-1}.

The number of transferred electrons (n) can be obtained from the slope of the *Koutecký-Levich* diagrams at different potentials according to the equation [15]:

$$n = \frac{4I_r}{I_d + \frac{I_r}{N}} \ , \quad (1.2)$$

where

n – number of electrons transferred;

I_d – disk current, A;

I_r – ring current, A;

N – collection efficiency (≈ 0.24 – 0.5)

3. RESULTS AND DISCUSSION

3.1. Influence of carbonisation environment on material structure

Despite the fact that the production of AO from biomass has been widely described in recent years [6], [7], the formation mechanisms of the material obtained in the carbonisation process vary considerably depending on the reaction environment and temperature.

In the carbonisation process, the conditions determine the size and number of graphene layers, otherwise referred to as coherent scattering areas in the carbonisate. In turn, the size and orientation of the crystallites determine the texture and electrical conductivity of the material [8]. Pyrolysis carbonisate is characterised by low porosity, and its structure consists of elemental crystals separated by many slit-like pores, but these pores are filled and blocked by 'disorganised' carbon residues (coke) resulting from secondary condensation and carbonisation of pyrolysis products. During the activation process, the filled pores are opened and the porous structure of the material develops.

According to the results in Table 1, which show the yields under different carbonisation conditions, it can be concluded that the highest yield of carbonisate was achieved in HTK 170. By increasing the HTK temperature to 260 °C, the yield decreases from 69.1 % to 46.6 %. When carbonising the material in an inert gas environment (350 °C and 500 °C), the yields are significantly lower, the lowest yield after carbonisation is for cellulose 21.4 %. In turn, the highest carbon content after carbonisation is PirK500, for bio-oil and cellulose, 81.74 %, 81.27 % and 77.78 %, respectively, and PirK350 – 66.14 %.

The carbon content of the carbonisate after HTK increases with increasing HTK temperature from 170 °C to 260 °C (from 49.41 to 71.29 %). Carbonised sewage sludge contains only 60.58 % carbon, but unlike all other raw materials, it already contains 5.54 % nitrogen.

Biomass carbonisation is a complex process with many reactions that result in the formation of non-condensable gases, liquid products or bio-oil and a solid residue – carbonisate. However, the morphology and microstructure of biomass does not change significantly during the carbonisation process (up to 600 °C) [9]. Compared to pyrolysis, hydrothermal carbonisation reactions take place at relatively low temperatures under hydrothermal conditions. Most hemicelluloses are transferred from lignocellulose to water at a hydrothermal process temperature below 180 °C, but cellulose degradation becomes apparent when the hydrothermal temperature reaches 230 °C [10].

In the carbonisation process, the raw material is subjected to a process of thermal decomposition, which is characterised by the release of volatile components. In order to understand the effect of the carbonisation environment on the carbon structure, analytical pyrolysis was performed, which allows to evaluate the differences in the composition of carbonisate according to the relative composition of volatile products.

Table 1

Raw Material Carbonisation Conditions, Yield and Element Analysis

Raw material	Sample	Carbonisation, °C, h, environment	Yield from a.d. mass, %	C, %	N, %	H, %	O, %
Birch wood	PirK350	350, Ar	38.4	66.14	0.25	4.93	28.65
	PirK500	500	31.7	81.74	0.97	1.47	15.82
	HTK170-2st.	170, 2, water	69.1	49.41	0.24	5.38	44.97
	HTK200-2st.	200, 2, water	63.4	51.52	0.17	5.23	43.00
	HTK240-4st.	240, 4, water	49.1	69.80	0.33	1.17	28.70
	HTK250-2st.	250, 2, water	47.9	69.56	0.17	3.97	26.30
	HTK250-4st.	250, 4, water	46.6	71.23	0.18	3.96	24.63
	HTK250-6st.	250, 6, water	48.1	69.12	0.17	3.67	27.04
	HTK250-12st.	250, 12, water	49.2	78.87	0.17	4.10	22.68
	HTK260-2st.	260, 2, water	46.6	71.05	0.15	4.85	23.95
Cellulose	C	500, 3	21.4	77.78	0.42	3.48	18.32
CRN sludge	SD	500, 4, Ar	30.2	60.58	5.54	3.01	30.87
Bio-oil – LG	BL	500, 2, Ar	26.9	81.27	0.18	1.82	16.73

The identified decomposition products of wood, its pyrolysis (PirK350, PirK500) and HTK (170, 200, 250 (2, 4, 6, 12 h), 260 °C) carbonisates were divided into three groups: 1 – decomposition products of carbohydrates, 2 – lignin degradation products, 3 – volatile products, such as $CO_2 + H_2O + CH_3OH$ (Fig. 2).

According to the analytical pyrolysis data, the carbohydrate content (~ 50 %) of volatile products in the raw wood sample, as well as PirK350, HTK170 and HTK200 carbonisate, is similar (see Fig. 2) and the carbon content after carbonisation is low (Table 1) which indicates an incomplete carbonisation process. In turn, the carbon content in PirK500 and HTK250 (Table 1) is higher and the ratio of lignin to carbohydrate derivatives (L / C) in volatile products (Fig. 2) increased rapidly with increasing carbonisation temperature.

In addition, unlike pyrolysis coal, hydrothermal carbon contains more functional groups, such as hydroxyl and carboxyl groups, suggesting that the formation of a solid product in hydrothermal carbonisation occurs by a different mechanism. This can be observed from the results of elemental analysis because the obtained carbonisate from HTK contains more oxygen (Table 2). At a constant HTK carbonisation temperature, the composition of the elements practically does not change when the reaction time is changed [11].

Using N_2 adsorption isotherms at 77 K, the specific surface area (according to BET theory), total pore volume, micropore volume (DR), and pore width for carbonised materials were calculated for the obtained OM (Table 2). In the case of the considered carbonisates, the specific surface area is very low, but it increases with increasing carbonisation temperature. HTK250 4 h and 12 h. The total pore volume (113–114 mm^3 / g) is half that of PirK500 (226 mm^3 / g), the micropore volume is almost 10 times smaller (12–17 mm^3 / g and 105 mm^3 / g) and the average pore width is almost 7 times higher (9.4–9.9 nm and 1.4 nm).

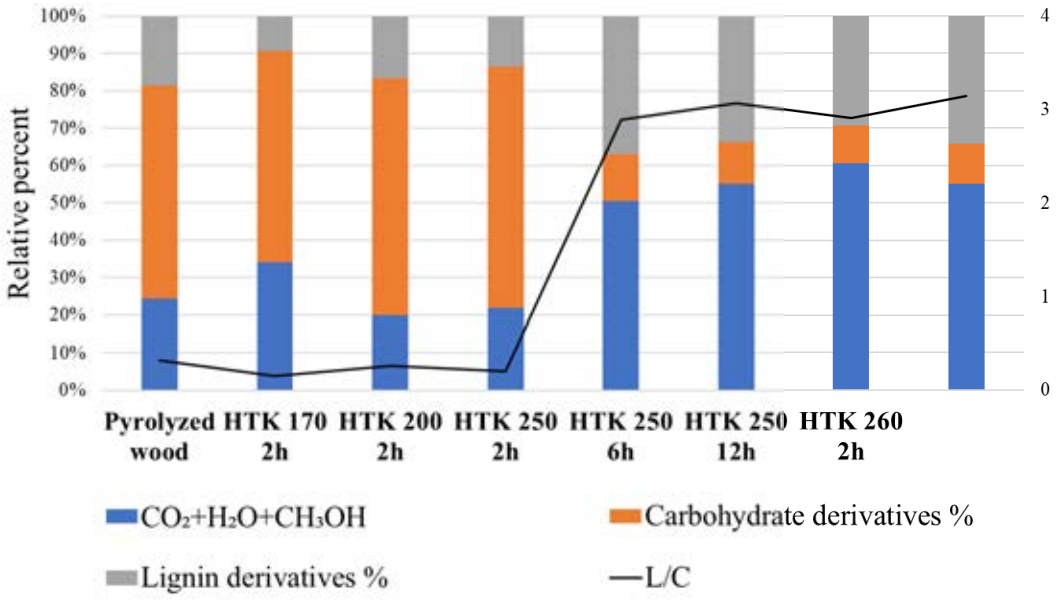

Fig. 2. Relative volatile product content and lignin / carbohydrate ratio (L / C) of analytical pyrolysis of wood, pyrolysed wood (350 °C) and hydrothermal carbonised wood (170°C, 200°C, 250°C (2, 4, 6, 12 hours), 260 °C).

Table 2

HTK250-4 h and 12-h Comparison of PirK500 specific surface area, total pore volume, micropore volume (DR) and pore width depending on carbonisation conditions

Samples	**Special surface (BET), m^2/g**	**Total pore volume, mm^3/g**	**Micropore volume (DR), mm^3/g**	**Pore width, nm**
HTK250-4h	4.2	113	12	9.4
HTK250-12h	4.6	114	17	9.9
PirK500	279	226	105	1.4

Examining and comparing the microphotographs of wood carbonisate and raw materials (Fig. 3 b), c), d)), it can be concluded that after carbonisation the hierarchical structure of wood is partially preserved. As a result of the HTK process, the degraded cellulose and hemicellulose products react with each other and condense on the surface of wood particles (Fig. 3 b)), but during pyrolysis, the wood cell walls remain smooth, the pores fill with carbonisation products of pyrolysis products and increase the temperature from 350 °C to 500 °C, they remain brittle (Fig. 3 c), d)).

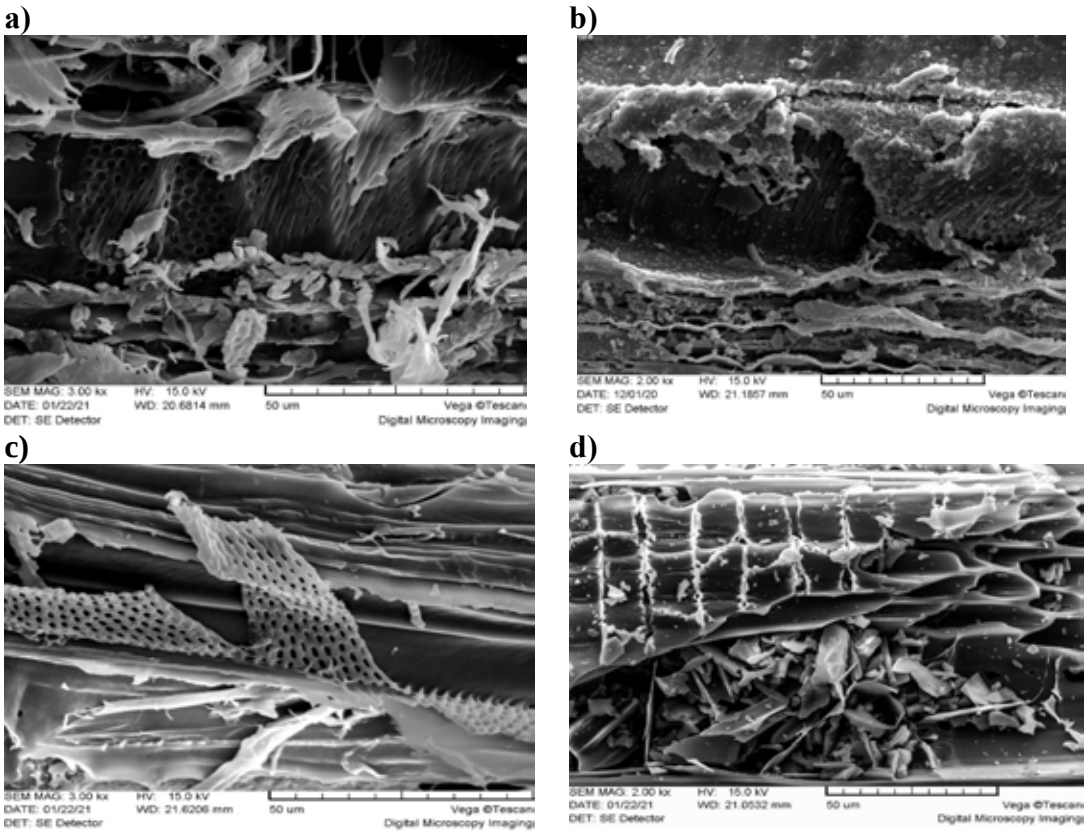

Fig. 3. SEM microphotographs: a) – wood; b) – HTK250; c) – PirK350; d) – PirK500.

3.2. Changes in porous structure during activation

In order to determine the effect of thermochemical activation parameters on the porous structure, wood char produced in SIA "Fille 2000" Latvia was activated with NaOH, using different amounts of activators and activation temperatures. In order to compare the structure of AO, various biomass-derived starting materials were activated at the activator-wood char ratio of 3 and the activation temperature of 700 °C (Table 3), as well as by subsequent testing of the porous structure and properties (Table 4).

The mechanism of interaction of chemical activation agents has not been fully elucidated, however, it is known that activating agents react with oxygen-containing functional groups with practically little effect on stable aryl-aryl C-C bonds. During the activation process, a number of wood-specific compounds, carbon oxides and hydrogen are formed [12]. The structure of the carbonate and the oxygen-containing functional groups (see Table 1 for the amount of oxygen) are the parameters that affect the activation efficiency. The more oxygen the material contains, the more efficient the activation. During the activation process, Na + ions interact with oxygen-containing functional groups located on the surface of carbon crystallite planes [13].

According to the results in Table 3, the highest AWC yield was achieved using the amount of activator K = 2 and the activation temperature 600 °C (based on wood – 15.0 %) and the lowest – using the amount of activator K = 3 and the activation temperature 800 °C (calculated

on wood – 6.1 %). This means that by increasing the amount of activator and the activation temperature, the yield of AO in them decreases. On the other hand, under constant activation conditions (T_{akt} = 700, K = 3), for different raw materials, the highest AO yield was achieved using HTK birch wood as a precursor (9.2 %). The lowest yield was obtained using black liquor as a raw material (5.93 % and 2.27 %).

Table 3

Carbonisation, Activation Conditions and AO Yield Based on Different Raw Materials

Raw material	**Sample**	**K**	**Activation, °C**	**Yield from a.d raw material mass, %**	**O, %**
Wood char	AWC-2-700	2	700	11.3 [1]	4.46
	AWC-3-600	3	600	9.9 [1]	5.51
	AWC-3-650	3	650	8.7 [1]	3.96
	AWC-3-700	3	700	7.9 [1]	3.37
	AWC-3-750	3	750	6.4 [1]	3.09
	AWC-3-800	3	800	6.1 [1]	2.25
	AWC-4-700	4	700	8.0 [1]	3.15
Cellulose	AC	3	700	7.3	5.77
Black liquor [2]	AMA	1	700	5.9	7.21
CRN sludge	ASD	2	700	9.3	6.43
Birch wood chips	AHTK (HTK-250-4h)	3	700	9,2	6.91
Bio oil-LG	ABL	3	700	7.0	5.99

[1] Yield from a.s wood mass

[2] Raw material was not carbonised prior to activation

K – Mass ratio of NaOH to carbonisate

The SEM results have shown that the particles of AWC samples obtained after thermal carbonisation of wood have a layered structure (Fig. 4 d)), while the AHTK particles obtained after hydrothermal carbonisation of wood have a flaky structure (Fig. 4 c)). The structure of the carbonisate obtained by hydrothermal carbonisation is less dense than the structure of the pyrolysis carbonisate. Therefore, much greater movement of molecules and ions is possible during activation. Reactions of sodium ions and oxygen-containing functional groups in carbonisates lead to the cleavage of bonds between adjacent layers, as well as the formation of new – C-C- bonds. During HTK activation, the bonds are broken more easily and the plates separate from each other. In the case of thermal carbonisation, the structure of wood char is denser and the bonds are stronger. In addition, the reduced metallic sodium formed during the activation process enters the system and forms carbonate salts between the crystallite layers, and after the demineralisation process, when the Na salts are washed away, pores are formed [14].

In order to achieve an optimal AO pore structure, it was important to find out how it is affected by the raw material used and its carbonisation conditions. For this purpose, the porous structure of carbon was studied before and after activation. As the obtained N_2 adsorption isotherms show, the porous structure changes depending on the raw material (Fig. 5). Prior to activation, carbonates have a relatively low specific surface area and porosity.

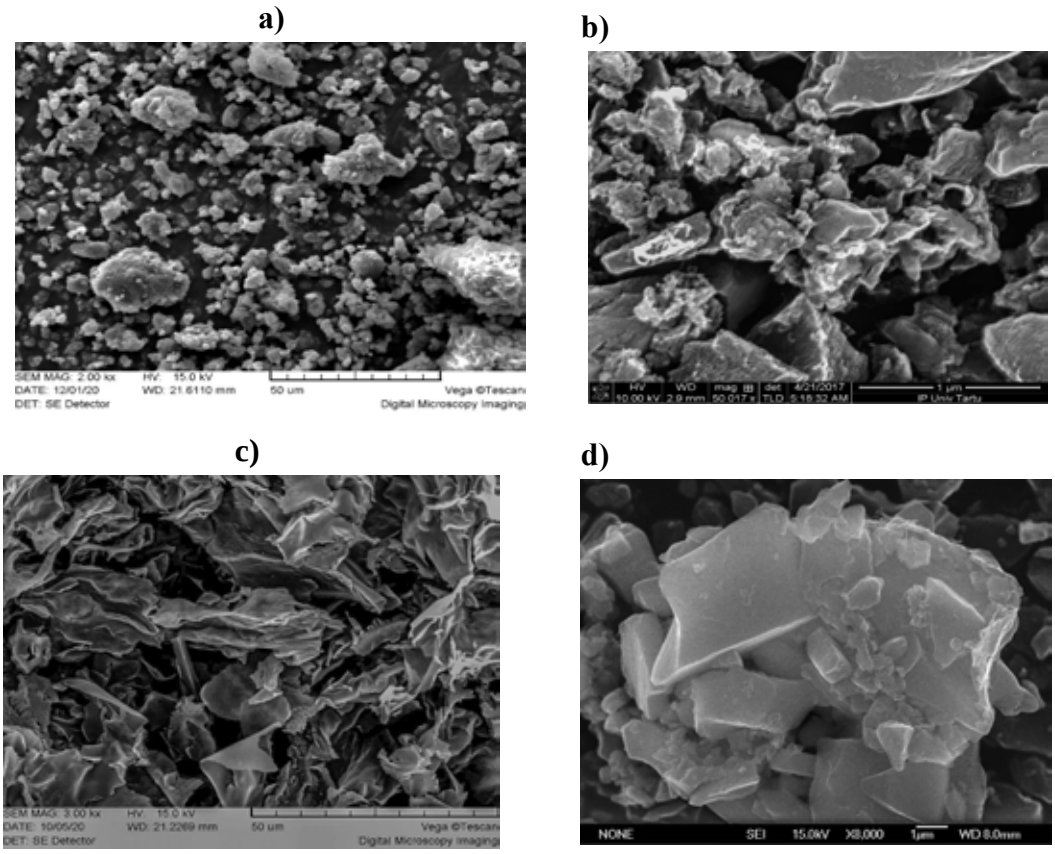

Fig. 4. SEM microphotographs: a) – HTK carbonisate ; b) – WC; c) – AHTK; d)– AWC; AO obtained at 700 °C and K = 3.

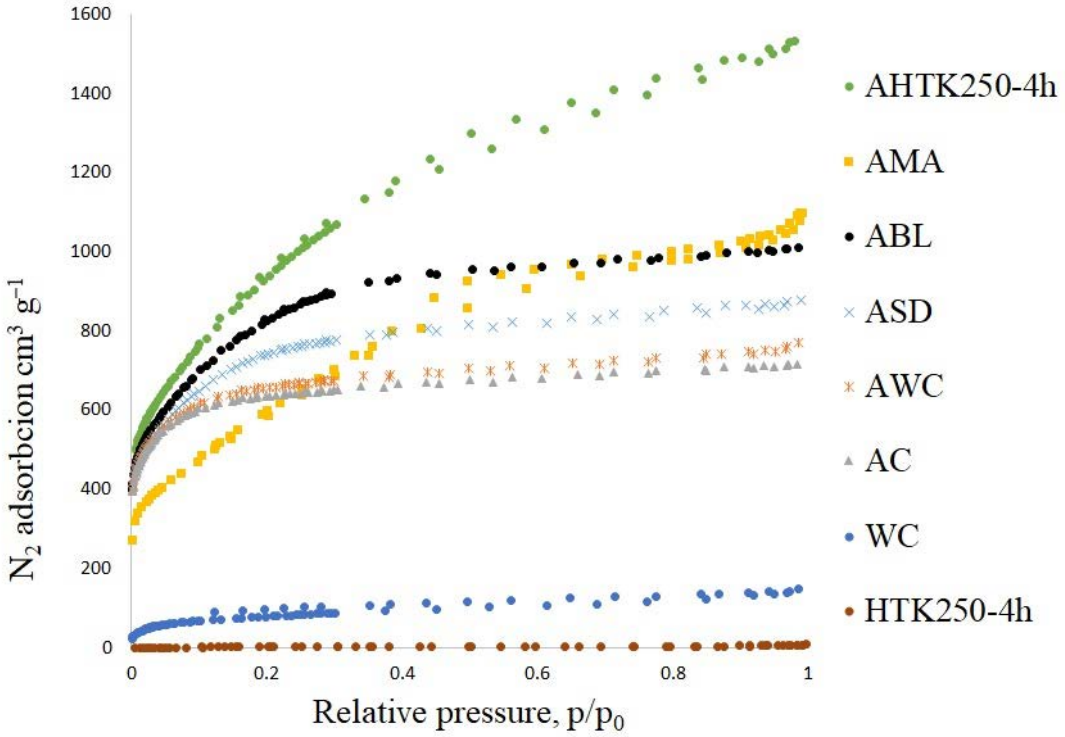

Fig. 5. Adsorption isotherms of carbonisates and activated carbon (K = 3, T_{akt} = 700 °C).

Judging by the slope of the adsorption isotherms, the adsorption of AO from wood char, cellulose, sewage sludge and bio-oil corresponds to type I isotherms (see Fig. 5), which are characteristic of carbons containing mainly micropores.

The slope of the isotherms of AO obtained by activating HTK carbonisate or black liquor differs from the isotherms of a typically microporous material. According to Dubiņina-Radušķevičs' theory, adsorption of micropores takes place according to the volume filling mechanism, but in the presence of mesopores at relative nitrogen pressure exceeding 0.4, adsorption takes place according to the polymolecular condensation mechanism [15], [16].

Porous structure parameters were calculated for the AWC samples obtained using N_2 adsorption (Table 4). According to the results in Table 4, the total specific pore volume AWC increases with increasing activator amount and activation temperature, reaching a maximum of 1.52 cm^3/g K = 3 cases at activation at a temperature of 800 ºC. However, it is important to note that according to the DR theory, which evaluates only the micropore volume, it can be seen that this indicator changes less linearly and starts to decrease at higher activation temperatures, possibly due to micropores merging into larger pores, because according to the Table 4 results their size is increasing. Calculating the mesopore volume, it can be seen that it, like the total pore volume, increases with increasing activation parameters, reaching a maximum in the case of 0.66 cm^3/g K = 3 at an activation temperature of 800 ºC.

As the amount of activator increases and the temperature increases, the specific surface area increases in the case of all three theories, a similar trend was observed in the case of the total pore volume. The highest specific surface values for AWC samples, according to BET theory, were obtained in the case of K = 3, while activation at 700 °C led to the maximum specific surface value of 2845 m^2/g, however, at lower temperatures the results decreased significantly (~ 2300 m^2/g 600 °C temperature). The highest specific micropore surface area was achieved at K = 3 and activation at 650 °C and 700 °C is the same, 2735 m^2/g and 2726 m^2/g, respectively.

Calculations of nitrogen adsorption isotherms show that the porosity of AWC, AC, ASD and HDL consists mainly of micropores with a volume of 0.79–0.99 cm^3/g, an average width L0 of about 1 nm and a small mesopore volume. In turn, the porosity of AMA and AHTK is formed by both micropores (Vmicro 0.88–1.07 cm^3/g) and mesopores (Vmezo 0.91–1.44 cm^3/g). The volume of mesopores in AHTK samples increases with increasing HTK duration from 1 to 6 hours and temperature from 200–250 °C and reaches a maximum of 1.44 cm^3/g.

By regulating the activation parameters, and thus also the porous structure, it is possible to select the most suitable AOs for use as feedstocks for the production of ORR catalysts for fuel cells. The ORR performance of a carbon material depends on the number of active centres and key properties such as specific surface area and pore size distribution [17], [18]. For example, a high specific surface area and a suitable pore size distribution can provide a sufficient number of active centres and, accordingly, ensure a rapid mass transfer [19], [20]. In addition, for porous carbon materials, it has been shown that a small mesopore volume and a large micropore volume would create a high charge transfer resistance, reduce the potential for mass transfer and the use of active centres. In turn, excessive mesopore volume and small micropore volume

can significantly reduce ORR active centres and porous surface [21], [22]. Therefore, an optimal pore size distribution must be ensured in the carbon structure to ensure maximum mass transfer and reduce charge transfer resistance.

Table 4

AO Porous Structure Parameters Based on Different Raw Materials

Sample	Pore volume, cm^3/g				Micropore width, nm	Specific surface, m^2/g		
	$V_{kop.}$	$V_{mikro\ (DR)}$	V_{mezo}	V_{DFT}	L_{DR}	S_{BET}	S_{DR}	S_{DFT}
AWC-2-700	1.18	0.88	0.30	1.00	1.36	2295	2514	1768
AWC-3-600	1.20	0.94	0.26	1.06	1.35	2333	2642	1871
AWC-3-650	1.34	0.92	0.42	1.19	1.42	2699	2735	1917
AWC-3-700	1.42	0.99	0.49	1.23	1.42	2845	2726	1944
AWC-3-750	1.43	0.87	0.56	1.29	1.35	2750	2454	1833
AWC-3-800	1.52	0.86	0.66	1.37	1.37	2733	2429	1813
AWC-4-700	1.51	0.83	0.68	1.36	1.50	2696	2333	1614
ABL	1.23	0.81	0.28	0.95	1.33	2209	2454	1715
AC	1.35	0.93	0.42	1.21	1.36	2728	2623	1919
ASD	1.31	0.86	0.45	1.18	1.36	2429	2418	1756
AMA	1.79	0.88	0.91	1.63	1.50	2770	2474	1817
AHTK-250-4h	2.11	1.02	1.09	2.17	1.47	3465	3019	2274

The pore distribution is influenced by several factors: the starting material and its carbonisation conditions (temperature, reaction time and environment), the amount of activator and the activation temperature.

As can be seen in Fig. 3 a), b), increasing the activation temperature and/or the amount of activator in the AWC samples, mesopores with a size above 2 nm appear and their volumes and dimensions increase with increasing activation parameters (from 2–3 nm at 650 °C to 2–4.5 nm at 800 °C and 2 nm at K = 2 to 3.5 nm K = 4). With the appearance of mesopores, the specific surface areas of the samples decrease, especially according to the DR theory, because it characterises the specific surface area of micropores.

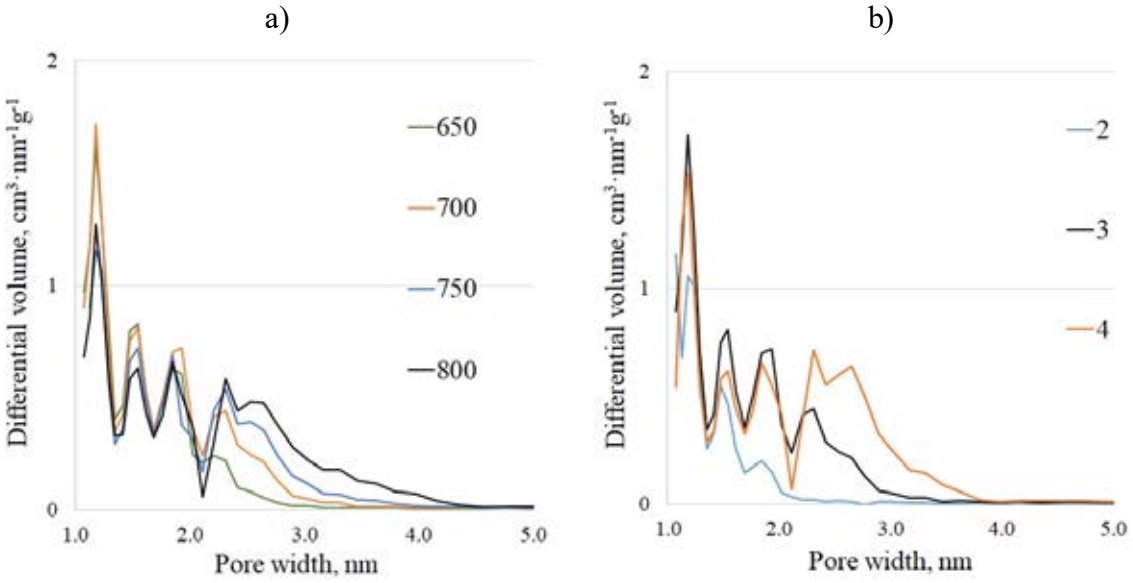

Fig. 6. Pore size distribution in AWC samples depending on: a) activation temperatures (K = 3); b) the amount of activator (K = 2;3;4 and T_{akt} = 700).

Comparing the AWC, ABL, AMA and AHTK samples (Fig. 7) it can be seen that the ABL pore size distribution is similar to the AWC sample, only with a smaller pore volume, but the AMA and AHTK sample has more mesopores with a size of 2–4.5 nm.

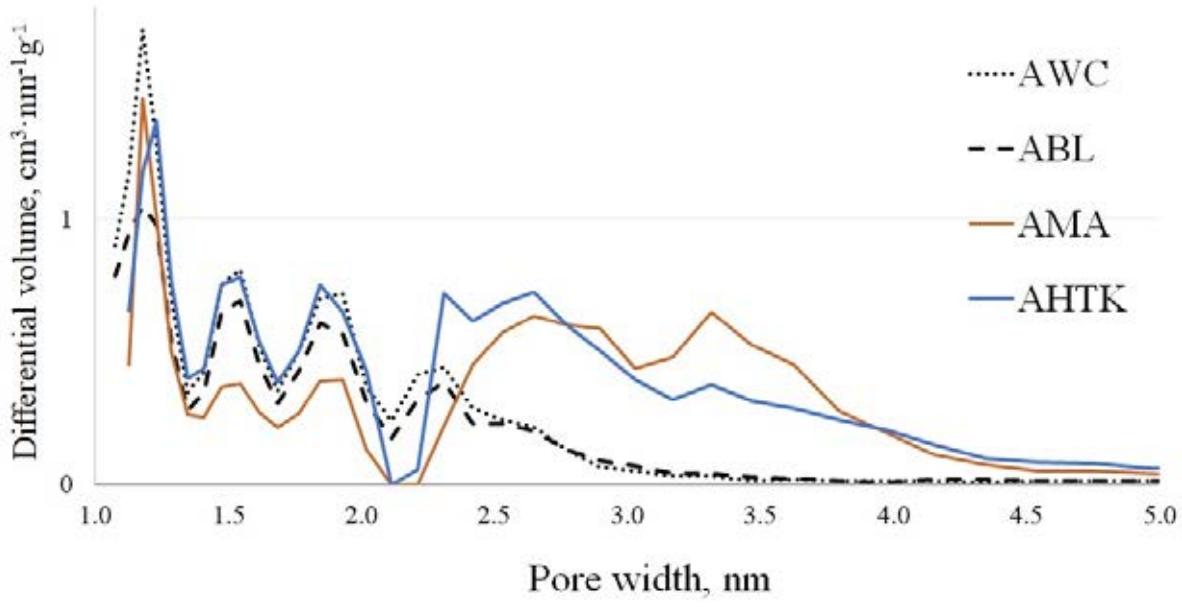

Fig. 7. AMA (T_{akt} = 700; K = 2), AWC (T_{akt} = 700; K = 3) and ABL (T_{akt} = 700; K = 3) sample pore size distribution.

3.3. Changes in the structure of activated carbon after doping with nitrogen

N-doping is a modification of the carbon structure by introducing nitrogen into it while activating the adjacent carbon atoms, which form active centres and thus improve the electrochemical properties of the material. Nitrogen was introduced into the structure using two different methods and reagents, followed by heat treatment at 800 °C or 950 °C.

Table 5

Elemental Analysis of N-doped Wood Char and AO Based on Various Precursors

Raw material	Processing conditions	N, %	C,%	H, %	O, %
WC	DMF[1], DCDA[2] 700[3]	20.67	73.84	1.00	4.49
AWC	3,600[4]- DMF[1], DCDA[2],800[3]	7.52	89.53	0.68	2.27
	2,700[4]-DMF[1], DCDA[2],800[3]	4.26	92.33	0.63	2.78
	3-650[4]- DMF[1], DCDA[2],800[3]	6.72	91.12	0.70	1.46
	3,700[4]- DMF[1], DCDA[2],800[3]	5.55	90.97	0.89	2.59
	3-750[4] - DMF[1], DCDA[2],800[3]	3.42	93.08	0.72	2.79
	3,800[4]- DMF[1], DCDA[2],800[3]	3.66	93.98	2.06	0.30
	4,700[4]- DMF[1], DCDA[2],800[3]	5.47	86.75	0.73	7.05
	3,700[4]-MEL[2],800[3]	4.3	91.47	0.2	4.03
	3,700[4]-MEL[2],950[3]	2.41	94.39	0.18	3.02
AC	3,700[4]- DMF[1], DCDA[2],800[3]	4.42	94.81	0.46	0.31
	500[5]-2,700[4]-DMF[1], DCDA[2],800[3]	6.78	89.67	0.63	2.92
AMA	2,700[4]- DMF[1], DCDA[2],800[3]	6.51	80.98	0.76	11.75
AHTC	250,4st[4] -3,700[4]- DMF[1], DCDA[2],800[3]	5.31	90.05	1.81	2.83
	250,4st[5] -3,700[4]-MEL[2],800[3]	5.78	91.23	1.65	1.34
	250,4st[5] -3,700[4]-MEL[2],950[3]	2.89	93.92	1.54	1.65
ABL	3,700[4]- DMF[1], DCDA[2],800[3]	5.61	90.4	1.44	2.55

The nitrogen content entered is affected by the structure of the material before doping (Table 5). By performing doping before activation, it is possible to inject the highest amount of nitrogen (15–20 % by weight) into the wood char, but under the same conditions, it is possible to inject a significantly lower amount of nitrogen (1–9 % by weight) into AO. By increasing the chemical activation temperature, the amount of activator and the doping temperature, the nitrogen content decreases after doping. This can be explained by the fact that the doping reagent reacts with the surface groups of the AO and the nitrogen replaces the oxygen, forming chemical bonds with the carbon-containing structural elements. The oxygen content of AO decreases (Table 3), increasing the activation temperature and the amount of activator, as well

[1] Solvent in which dicyandiamide is dissolved
[2] Doping reagent
[3] Doping temperature
[4] Carbonation conditions

as changes depending on the raw material. If DCDA was used as a doping agent, the best results for AWC samples were obtained at a ratio of K = 2, an activation temperature of 600 °C and a ratio of DCDA to the carbon of 20: 1 at a doping temperature of 800 °C (9.93 %, Table 5). By increasing the amount of activator to K = 3 and the activation temperature to 800 °C, lower nitrogen content was obtained under the same doping conditions (2.48 %, Table 5).

It is known from the literature [23] that using melamine as a doping reagent requires a higher doping temperature, therefore $AWC_{MEL}800$ and $AHTK_{MEL}800$ were reheated to 950 °C. As the doping temperature increased from 800–950 °C, the nitrogen content also decreased from 4.3 % to 2.4 %.

In Fig. 8 a), carbon, nitrogen and oxygen peaks can be distinguished in the X-ray photoelectron spectroscopy (XPS) report wide-scan spectra. Compared to the carbon peak, the intensity of the nitrogen and oxygen peaks is low and decreases with increasing AO activation temperature. This is due to the fact that most of the N-doped activated carbon consists of carbon (~90 %) and its content increases with increasing activation temperature. In turn, the amount of nitrogen injected decreases with increasing activation temperature.

Opinions on the activity of nitrogen in the structure of carbon material are still controversial. Some groups of scientists believe that high nitrogen content on the surface is the main factor in achieving high electrochemical activity [24], [25], while others have not found a correlation between nitrogen content and electrochemical activity [26], [27], [28]. To determine the form of nitrogen, the N1s peaks (Fig. 8 b)) were deconvolved using Gaussian lines of equal width. Most of the nitrogen was found to be in the pyridine (399.2 eV) and pyrrolic (401.2 eV) forms, and a small amount was found in the graphitic form (402.4 eV) as well as nitrogen in the oxide form (405 eV).

a) b)

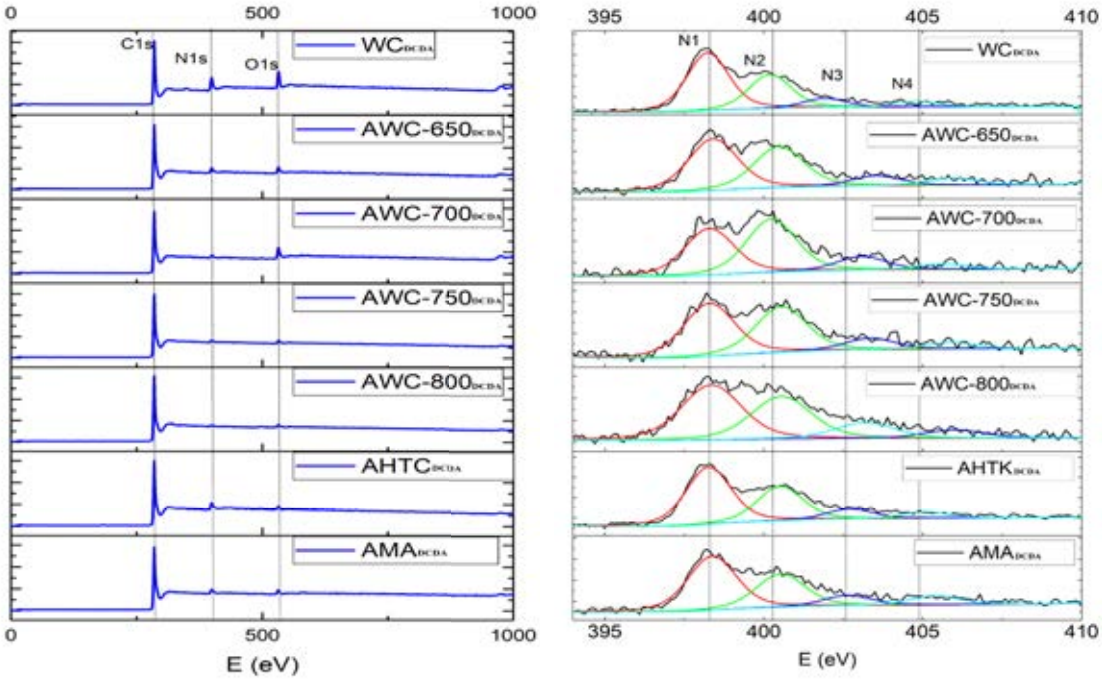

Fig. 8. N-doped activated carbon XPS: a) wide-scan spectra; b) N1s spectra.

Table 6 summarizes the effects of different starting materials and doping reagents on the distribution of nitrogen groups. After doping, the content of nitrogen forms obtained with DCDA in N-doped activated carbon changes with the change of starting material. For AWC samples obtained at different activation temperatures, the nitrogen content in the pyridine form increases with increasing activation temperature from 700–800 °C and reaches 48 % at 800 °C. In contrast, for AHTK and AMA samples at 800 °C, it is higher, 53 % and 50.5 %, respectively.

Table 6

Distribution of Nitrogen Groups on the Surface of N-doped Activated Carbon

Raw material	**Doping reagent**	**Pyridine-N, %**	**Pyrrole-N, %**	**Graphitic-N, %**	**N=O, %**
WC	DCDA	54.0	32.0	8.5	5.5
AWC-3-650	DCDA	47.0	37.0	9.0	7.0
AWC-3-700	DCDA	39.0	45.0	11.5	4.5
AWC-3-750	DCDA	45.0	39.0	10.0	6.0
AWC-3-800	DCDA	48.0	36.0	9.0	7.0
AWC-3-700	MEL	50.0	28.0	14.0	8.0
AHTK-3-700	DCDA	53.0	32.0	9.0	6.0
AHTK-3-700	MEL	53.0	30.0	10.0	7.0
AMA-2-700	DCDA	50.5	31.0	10.0	8.5

3.4. Use of doped activated carbon in the oxygen reduction reaction (ORR)

The oxygen reduction reaction (ORR) is the main reaction in fuel cells. Nitrogen-doped OM materials as non-metallic catalysts show high electrocatalytic activity in oxygen reduction reactions, making them one of the most promising alternative materials to replace expensive Pt catalysts. There are many publications reporting that the introduction of nitrogen into the carbon structure improves the ability of OM to reduce oxygen [6], [14], [15].

Figure 9 compares the oxygen reduction voltammetry curves of AWC samples before and after doping. The initial potential (–0.25 V AWC and –0.20 V AWC_{DCDA}) and half-wave potential (–0.32 V AWC and –0.30 V AWC_{DCDA}) of the AWC_{DCDA} sample are slightly more positive compared to the AWC sample, but with diffusion the limited current density reaches slightly lower values (–2.1 AWC and –2.4 AWC_{DCDA}), indicating that N-doping increases the properties of the catalyst. It should be noted that nitrogen only increases the activity of the catalyst because the amount of active centres is provided by a sufficiently large surface area and the required mesopore volume is provided for ion transport.

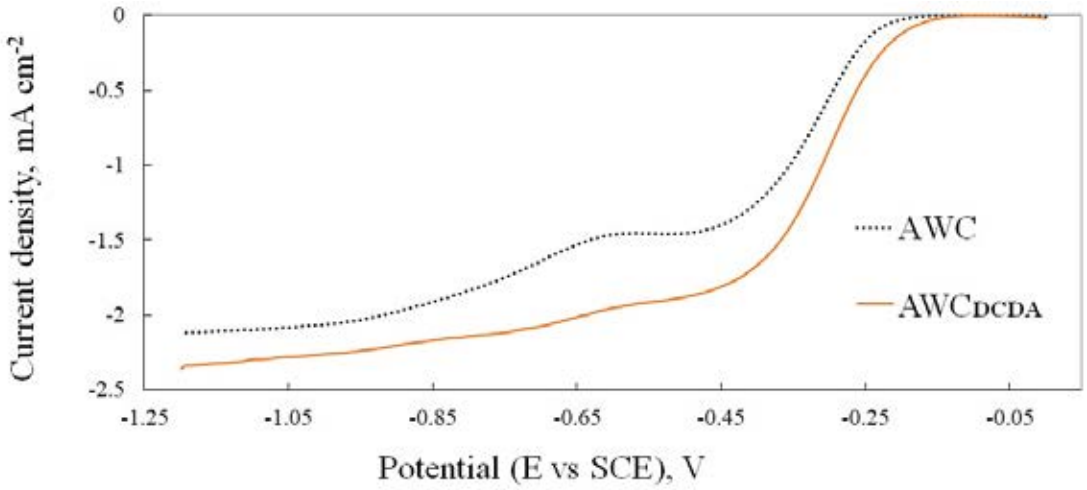

Fig. 9. Rotating disk electrode voltmetry curves for oxygen reduction for AWC samples (T_{akt} = 700 °C, K = 3) before and after N-doping with DCDA.

Influence of doped activated carbon sample raw material and activation temperature on ORR electrochemical characteristics

The electrochemical characteristics of ORR were studied in microporous AWC samples obtained under different activation conditions. ABL, AC, ASD and micro-mesoporous AHTK, AMA samples with different porous structure as well as nitrogen content and shape were also studied. Figure 10 compares oxygen reduction voltammetry curves for doped inactivated wood char sample (WC_{DCDA}) and AO DCDA samples from different feedstocks under constant activation conditions (T_{akt} = 700 °C; K = 3). Using ORR as a catalyst for WC_{DCDA}, ASD_{DCDA} and AC_{DCDA}, the initial potential (–0.25 V WC_{DCDA} and ASD_{DCDA}) and the half-wave potential (–0.31 V WC_{DCDA} and ASD_{DCDA}) remain virtually unchanged but become slightly more

positive for ABL_{DCDA} and AWC_{DCDA} (–0.20 V and –0.28 V), at the same time the diffusion-limited current density values decrease. The results obtained by ABL_{DCDA} are similar to the AWC_{DCDA} sample. The activity of WC_{DCDA}, ASD_{DCDA}, and AC_{DCDA} catalysts is lower than that of AWC_{DCDA}.

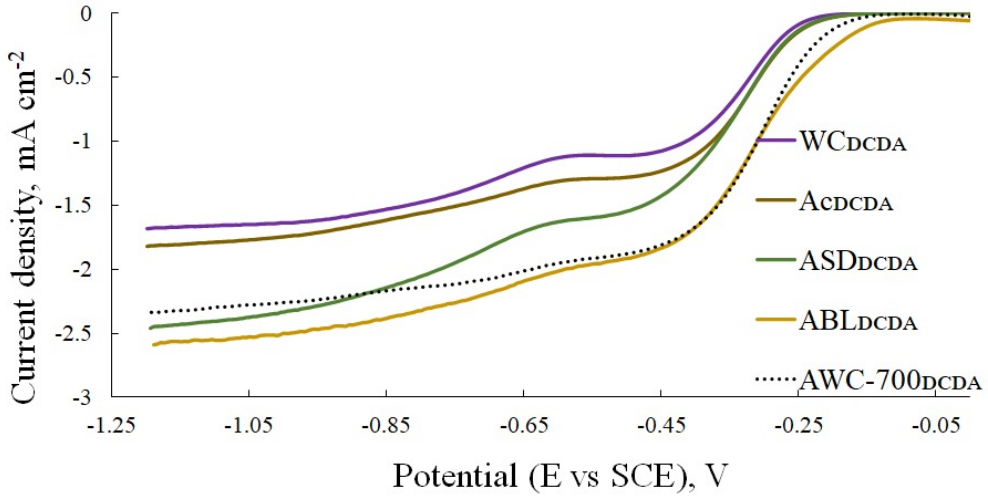

Fig. 10. Rotating disk electrode voltmetry curves for oxygen reduction on AO $_{DCDA}$ samples and N – doped wood char.

Figure 11 compares the oxygen reduction voltammetry curves AWC_{DCDA} (T_{akt} = 700, 750, 800 °C; K = 3), AMA_{DCDA}, (T_{akt} = 700 °C; K = 2), and $AHTK_{DCDA}$ (T_{akt} = 700 °C; K = 3) to draw conclusions about the effect of micro and mesoporous AO $_{DCDA}$ catalyst on the oxygen reduction reaction. ABL_{DCDA} and AWC 700_{DCDA} samples are microporous, while AWC 800_{DCDA}, AMA_{DCDA} and $AHTK_{DCDA}$ samples are micro-mesoporous. For them, the initial potential and the half-wave potential are practically unchanged, but at the same time, the values of the current density limited by diffusion decrease slightly and reach a minimum of –6.2 mA/cm^2 in the case of $AHTK_{DCDA}$.

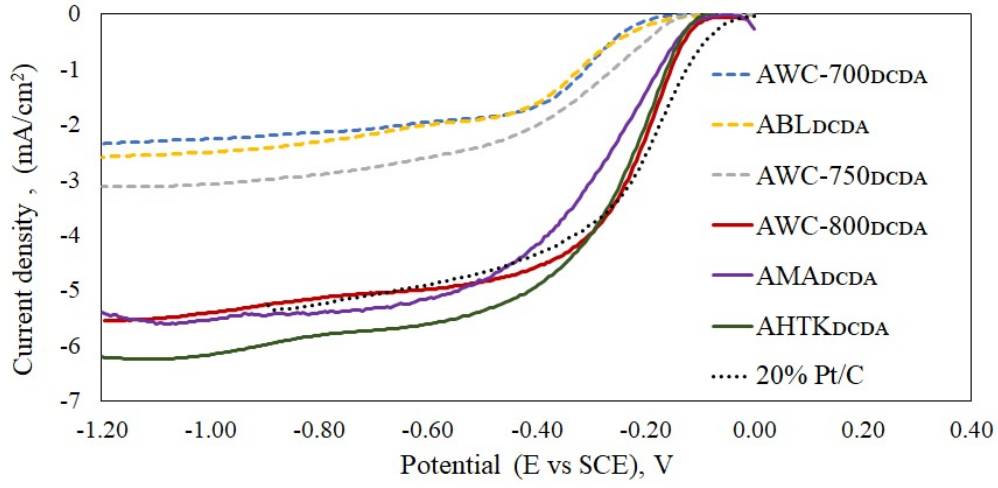

Fig. 11. Electrode voltmetry curves of the rotating disk of microporous and micro-mesoporous AO $_{DCDA}$ material for oxygen reduction.

The changes in the number of transferred electrons (per O_2 molecule) depending on the total pore volume, as well as the micropore and mesopore volume are shown in Fig. 12. As the activation temperature increases, the total pore volume increases linearly, as well as the mesopore volume and the number of transferred electrons increase linearly. For AMA_{DCDA} and $AHTK_{DCDA}$ samples, these parameters decrease slightly. The most efficient electron transfer occurs when the volume of mesopores (2.5–5 nm in size) is larger than the volume of micropores at a constant total pore volume.

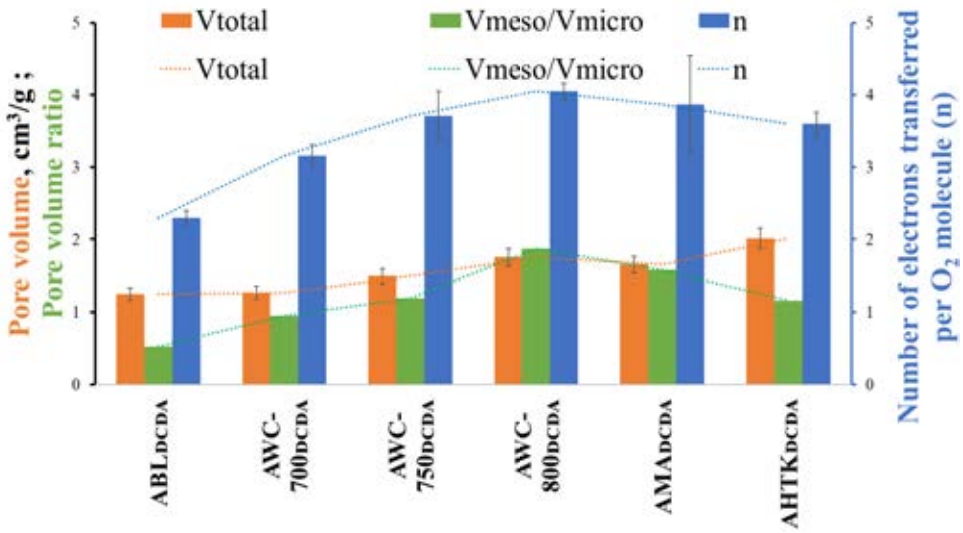

Fig. 12. Regularities of AO DCDA porous structure parameters and number of transferred electrons (n).

ORR characteristics of doped activated carbon samples depending on the doping reagent

To investigate the effect of doping reagent on the oxygen reduction reaction, Fig. 13 compares the oxygen reduction voltammetry curves for N-doped activated wood char (AWC_{DCDA}; AWC_{MEL}; AWC_{MEL}-950) and N-doped activated carbon by HTK ($AHTK_{DCDA}$; $AHTK_{MEL}$; $AHTK_{MEL}$-950) samples under constant activation conditions (Activation = 700 °C; K = 3). The lowest results were obtained by doping AHTK with MEL, because this doping method adversely affects the structure of the material. The initial potential and half-wave potential of AWC-NDCDA become slightly more positive than AWC_{MEL}-950, but the diffusion-limited current density reaches slightly lower values (–2.3 mA/cm^2-AWC_{DCDA}; –1.4 mA/cm^2-AWC_{MEL}-950). In contrast, the onset potential and half-wave potential of the $AHTK_{DCDA}$ sample become significantly more positive and the diffusion-limited current density reaches much lower values (–6.2 mA/cm^2-$AHTK_{DCDA}$; –2.3 mA/cm^2-$AHTK_{MEL}$-950) than when doping with MEL.

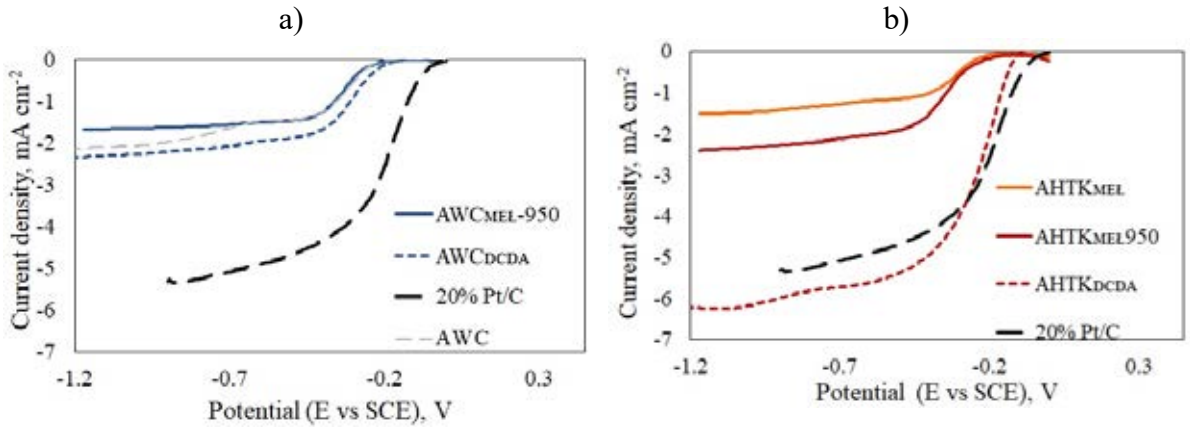

Fig. 13. Rotary disk electrode voltmetry ORR curves depending on doping agent and raw material: a) AWC-N samples and b) AHTK-N samples.

After the doping of the samples, the parameters of the porous structure of carbon materials also change. As it can be seen in Fig. 14, experiments with the AWC sample show that the use of MEL for impregnation reduces the porous structure slightly more than in the experiments using DCDA, but in both cases, they are lower than the starting activated carbon. The change in porous structure is greater when nitrogen is introduced into the structure of the AHTK. When DCDA is used, the specific surface area, total pore volume and micropore volume decrease similarly to AWC, but when MEL is used, the porous structure decreases by almost a third.

Compared to the MEL, samples using DCDA as a doping agent show much higher activity in the oxygen reduction reaction.

Based on the obtained results, possible doping mechanisms with DCDA and MEL were developed (Fig. 15). When DCDA is introduced into the carbon material structure, the reagent binds to the pore surface, whereas in the case of MEL, the reaction takes place mainly on the outer surface of the AO particle. As a result of MEL polymerization, part of the pores are clogged.

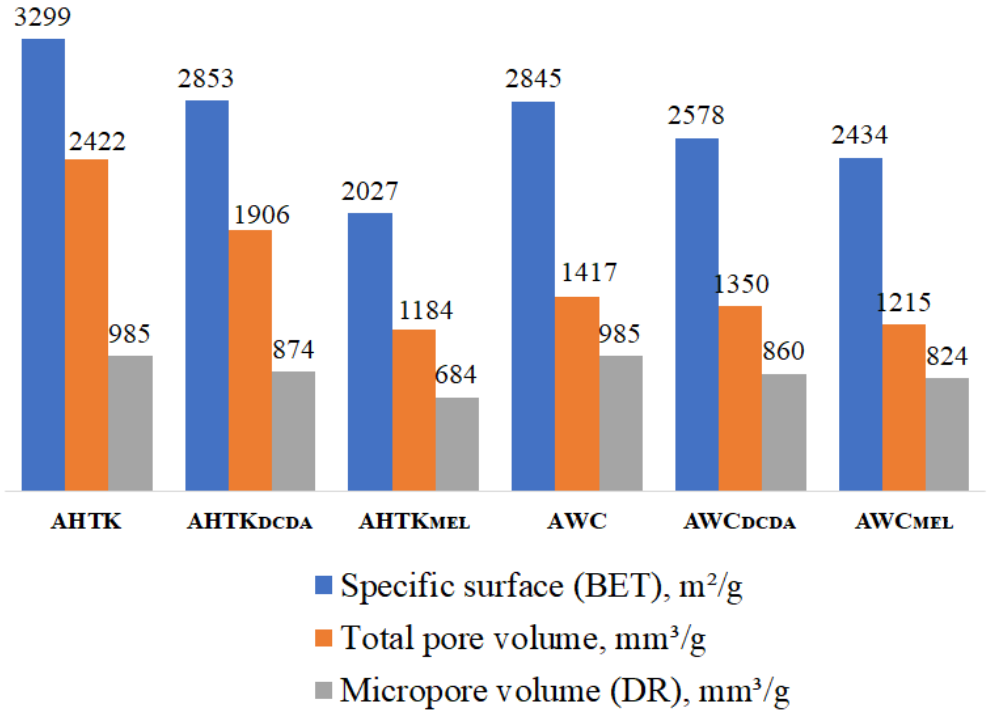

Fig. 14. Parametres of samples of porous structures AWC (K = 3; *T* = 700 °C and AHTK (*T* = 250 °C, 4 st.) before and after N-doping.

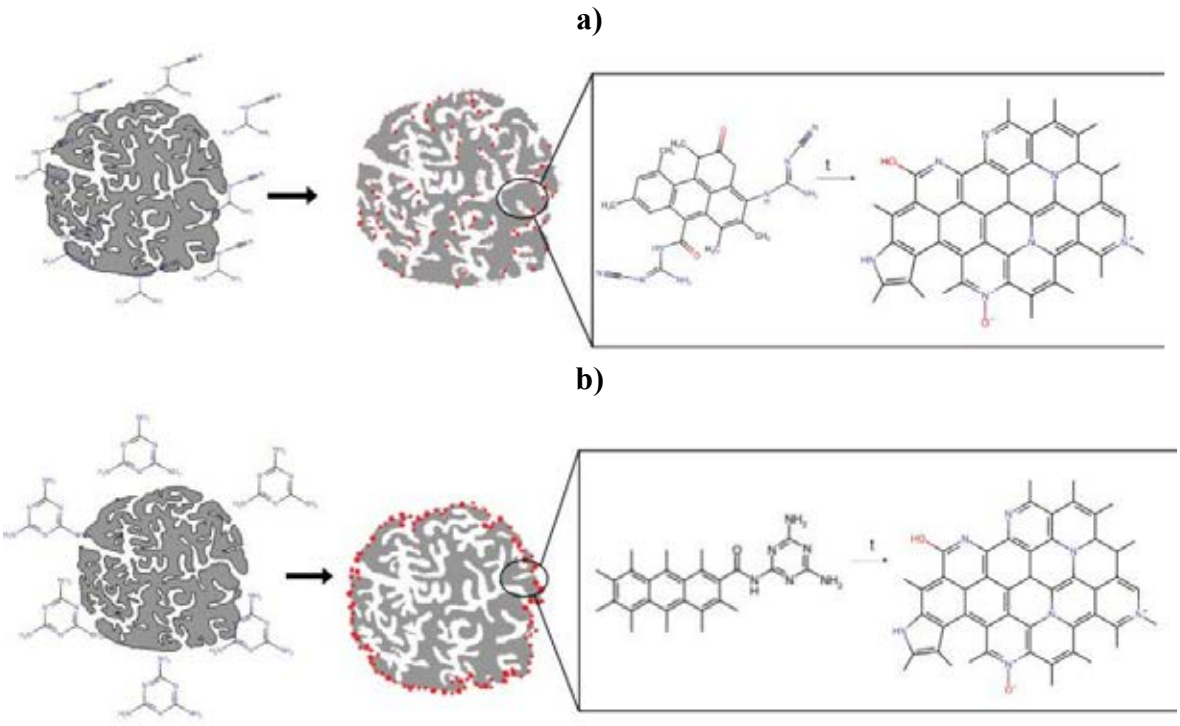

Fig. 15. Possible N-binding mechanism of doping reagents: a) DCDA and b) MEL. The red dots represent the binding sites of the doping reagent on the pore surface.

Influence of repeated heat treatment on electrochemical characteristics of ORR

In order to increase the electrochemical activity of AWC $_{DCDA}$, the samples were 'trained' using repeated heat treatment at 800 °C. Comparing the AWC $_{DCDA}$ (T_{akt} = 700 °C – 800 °C) ORR curves before and after repeated heat treatment, it can be seen in Fig. 16 that the catalyst activity increased. The initial potential becomes more positive and in the case of AWC-700DCDA-800 the offset is the largest, as a result of which the beginning of the curve practically overlaps with AWC-800$_{DCDA}$ (AWC-700$_{DCDA}$ E_{onest} = –0.17 V before repeated heat treatment and E_{onest} = –0.1 V after). The half-wave potential changes similarly, with the AWC-700$_{DCDA}$-800 gaining a slightly more positive value than the AWC 800$_{DCDA}$. Diffusion limited current density values decrease significantly and reach a minimum of –6.2 mA/cm^2 in the case of AWC-700$_{DCDA}$-800 (–2.3 mA/cm^2 before reheating). The activity of the AWC-750$_{DCDA}$-800 sample is higher, but the activity is significantly lower than in the case of the AWC-700$_{DCDA}$-800.

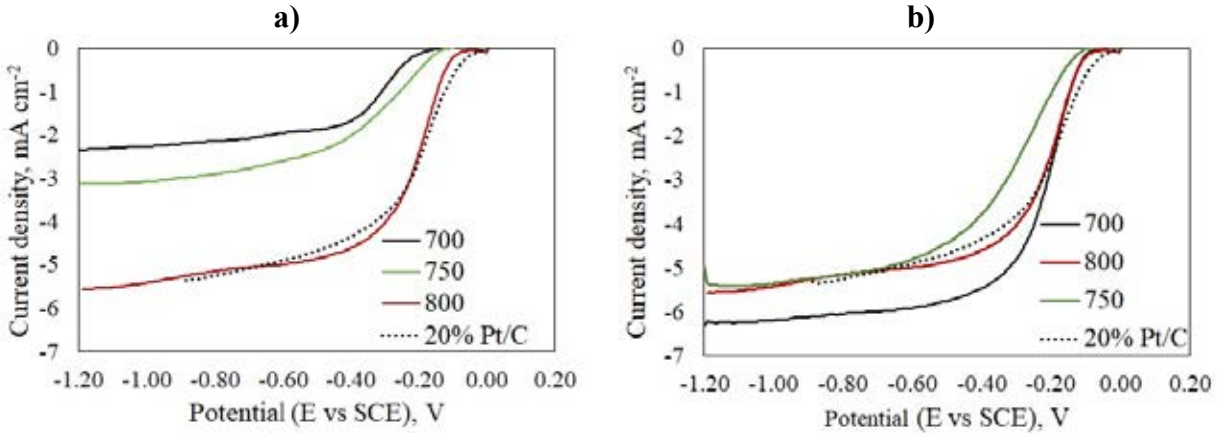

Fig. 16. Electrode voltmetry ORR curves of the rotating disk of AWC$_{DCDA}$ sample (T_{akt}: 600, 700, 750, 800 °C): (a) without further processing; (b) after repeated heat treatment at 800 °C .

During repeated heat treatment, the structure of the AWC-700$_{DCDA}$-800 catalyst changes due to a slight decrease in the specific surface area (before treatment – 2435 m^2/g; after heat treatment – 2245 m^2/g), because larger pores are formed when the pore walls break (L pre- 1.36 nm; after heat treatment – 1.63 nm) and the total pore volume increases (Vk before treatment – 1.27 cm^3 / g; after heat treatment – 1.34 cm^3/g) (Table 7). Reheating reduces the nitrogen content of AWC $_{DCDA}$ from 5.55 % to 2.75 %, resulting in an increase in pyridine N form from 39 % (AWC-700$_{DCDA}$) to 59 % (AWC-700$_{DCDA}$-800). Both theoretical calculations [29] and experiments with catalysts containing almost exclusively pyridine nitrogen [30] have shown that pyridine-N is the most active part of nitrogen. As almost half of the nitrogen in the AWC-700$_{DCDA}$-800 was in the form of pyridine, the effect is significant, although the total nitrogen content has decreased significantly.

As can be seen in the SEM microphotographs (Fig. 17 (a)), the AWC-700$_{DCDA}$-800 particles are divided into plates with a thickness of 50 by 20 nm under the influence of temperature, and the TEM photomicrographs (Fig. 17 (b)) show that the material consists of graphene lattice plate agglomerates and amorphous carbon areas with a porous structure. Some layered catalyst

particles have a thickness of 3.55 nm and the interlayer spacing between the two layers is ~ 0.35 nm, which indicates that some catalyst particles have a graphene-like structure [31], [32].

Table 7

Comparison of the Porous Structure of AWC-700$_{DCDA}$ Samples Before and after Repeated Heat Treatment

Sample	Special surface (BET), m^2/g	Total pore volume, mm^3/g	Micropore volume (DR), mm^3/g	Mesoporous volume, mm^3/g	Average pore width, nm	N, %	Pyridine N, %
AWC-700$_{DCDA}$	2435	1.27	0.86	0.41	1.36	5.55	39
AWC-700$_{DCDA}$-800	2245	1.34	0.82	0.52	1.63	2.75	59

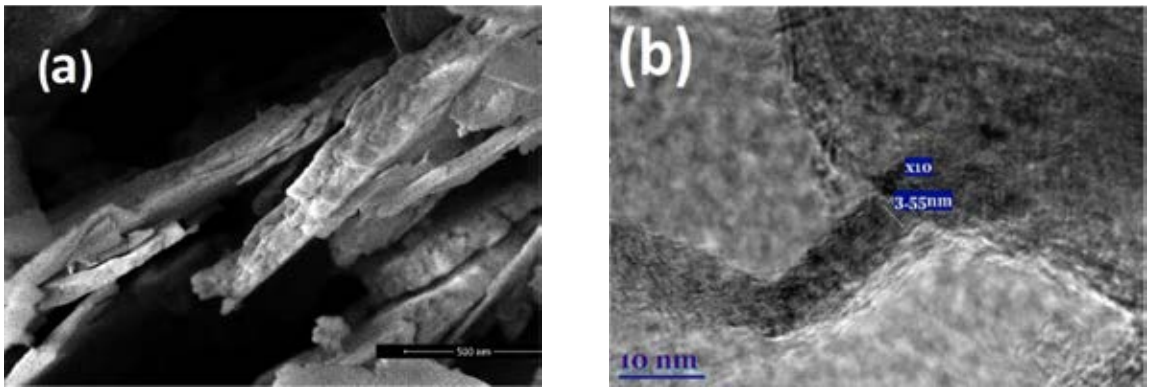

Fig. 17. AWC-N700$_{DCDA}$-800 microphotographs: a) SEM; b) TEM [Figure republished with the permission of *American Chemical Society* [33]].

Comparison of ORR catalyst activity

According to the experimental results, the oxygen reduction reaction activity of the catalysts decreases in the following order: DCDA-doped AO based on wood char (AWC-700$_{DCDA}$-800), DCDA-doped AO on wood char base (AWC800$_{DCDA}$), DCDA-doped AO on black liquor base (AMA$_{DCDA}$), DCDA-doped AO after HTK (AHTK$_{DCDA}$), DCDA-doped AO on wood char base (AWC750$_{DCDA}$), MEL-doped AO after HTK (AHTK$_{MEL}$-950), DCDA-doped AO on wood char base (AWC700$_{DCDA}$), DCDA-doped AO on bio-oil bases (ABL$_{DCDA}$), DCDA-doped AO on pulp mill sewage sludge bases (ASD$_{DCDA}$), DCDA-doped AO on cellulose bases (AC$_{DCDA}$), DCDA-doped wood char (WC$_{DCDA}$), MEL-doped AO on wood char base (AWC$_{MEL}$-950).

Of the obtained N-doped catalysts, ORR curves of four catalysts – AHTK$_{DCDA}$, AMA$_{DCDA}$, AWC-800$_{DCDA}$ and AWC700$_{DCDA}$800 practically coincide with the selected commercial 20 % Pt / C catalyst. Table 8 shows the electrochemical characteristics of the ORR, the porous structure, the nitrogen content and its form, as well as the yield from the absolutely dry mass of the raw material. For AHTK$_{DCDA}$, AMA$_{DCDA}$, AWC-800$_{DCDA}$ samples that have not been re-heat treated, the number of transferred electrons also increases with increasing meso to micropore ratio, reaching a maximum of 4.05 electrons in the case of AWC-800$_{DCDA}$. The

obtained results show that the most efficient electron transfer takes place in samples in which the mesopore volume of the material is larger than the micropore volume, keeping the total pore volume constant.

It should be noted that in the case of AWC-700_{DCDA}-800, pore distribution is not the main factor that improves the electrochemical properties. Repeated heat treatment at 800 °C for 'training' AWC-700_{DCDA} samples significantly improves the activity of the catalyst, and the number of electrons transferred per oxygen molecule is the largest – 4.6. Repeated heat treatment reduces the total nitrogen content but increases the content of pyridine N form to 59 %, which confirms that the pyridine-N form is the most active part of nitrogen in the catalytic oxygen reduction reaction.

Although the electrochemical activity of AMA_{DCDA}, AWC-800_{DCDA} samples is high, their yields from the absolutely dry raw material mass are relatively low 5.9 and 6.1 %, but the highest yield is $AHTK_{DCDA}$ 9.2 %.

Table 8

Nitrogen Content and Shape, Porous Structure Properties and Electrochemical Characteristics of ORR Electrocatalysts

Catalyst	**N, %**	**Pyridine-N form, %**	**Total pore volume, mm^3/g**	**V_{mezo}/V_{mic}**	**Number of e^- transferred (*n*)**	***J*, mA/cm^2**	**Yield from a.d. mass of raw material, %**
$AHTK_{DCDA}$	5.31	53.0	2.01	1.16	3.60	–6.22	9.2
AMA_{DCDA}	6.51	50.5	1.65	1.58	3.87	–5.35	5.9
$AWC800_{DCDA}$	3.66	48.0	1.75	1.87	4.05	–5.50	6.1
$AWC700_{DCDA}800$	2.75	59.0	1.34	0.63	4.60	–6.24	7.9

4. TEHCNOLOGY OF NITROGEN DOPED ACTIVATED CARBONS PRODUCTION

Based on the experiments performed and the results obtained, the principal technological line for the production of nitrogen-doped activated carbon (AO $_{DCDA}$) was developed, as well as the material and heat balances of the process was compiled. Our planned production volume of the experimental line is small – 1 t / year or 3.86 kg per day. At the same time, given that, for example, one Toyota Mira model with a power output of 113 kW requires 1.9 kg of doped activated carbon, future increase in demand is expected for such products.

Activated wood char, which is obtained from conventional wood char produced in Latvia, is intended to be used as a raw material for the production of AO DCDA, and the description of its extraction technology is given in A. Volpert's Ddoctoral Thesis [3], therefore, it is assumed that this coal will be produced in a separate plant. The cost of such activated carbon is relatively low and, according to our calculations, it is 16 EUR / kg, which is significantly lower than carbon nanomaterials and platinum.

The AO $_{DCDA}$ production process consists of the following steps:

1) impregnation of activated carbon with DCDA solution in DMF;

2) DMF distillation;

3) doping of activated carbon at 800 °C.

Technological scheme of AO $_{DCDA}$ production is shown in Fig. 18. 484 liters of DMF are loaded from the measuring tank (1) into the impregnation tank with the stirrer (2) and 78.7 kg of DCDA are added through the loading hatch; mixing is continued for another 15 minutes. Activated carbon (AO) is delivered from the warehouse in polyethylene bags, weighed 4.1 kg, loaded into an impregnation tank and the mixing is continued for another 30 minutes. The suspension is then fed automatically to a vacuum dryer with a mechanical stirrer and electric heating (3), where DMF is distilled off. The DMF is condensed in the cooler (4) and collected in a tank (5). From there it is returned to the impregnation process in the measuring tank (1) using a pump (8). The vacuum in the system is provided via an intermediate tank (6) with an oil-free vacuum pump (7).

The dry impregnated product (~83 kg) is mechanically unloaded through the unloading hatch at the bottom of the vacuum dryer in portions of ~8 kg in metal containers measuring 700 × 500 × 150 mm and transported further to a continuous tunnel kiln (9) for doping. The containers are fed into a continuous tunnel kiln, which is a stainless steel tunnel through which containers with a doping mixture move on rollers. Heating is realized with the help of electric heating elements. The kiln is divided into heating, doping and cooling sections, which are delimited by locks through which containers are periodically inserted and discharged. Containers are passed through the kiln by calculation to remain in the doping zone for 120 minutes at a temperature of 800 °C. The tunnel kiln is provided with an overpressure of argon flow from the tank (14) to prevent atmospheric air from entering the activation kiln when loading and unloading containers.

In the doping process, DCDA decomposes to form mainly ammonia, nitrogen oxides, carbon dioxide and some cyanides, while small amounts of carbon monoxide and dioxide are

derived from the oxygen-containing groups of activated carbon. Therefore, the stream of gases and vapors released during the process is introduced into a scrubber (10), where ammonia is neutralized with phosphoric acid, which is circulated by a pump (11) and replenished from the tank (13). The purified gas stream is then vented to the atmosphere through an adsorption column containing activated carbon (12). The finished AO $_{DCDA}$ product is packed in 10 kg packs and sent to the warehouse.

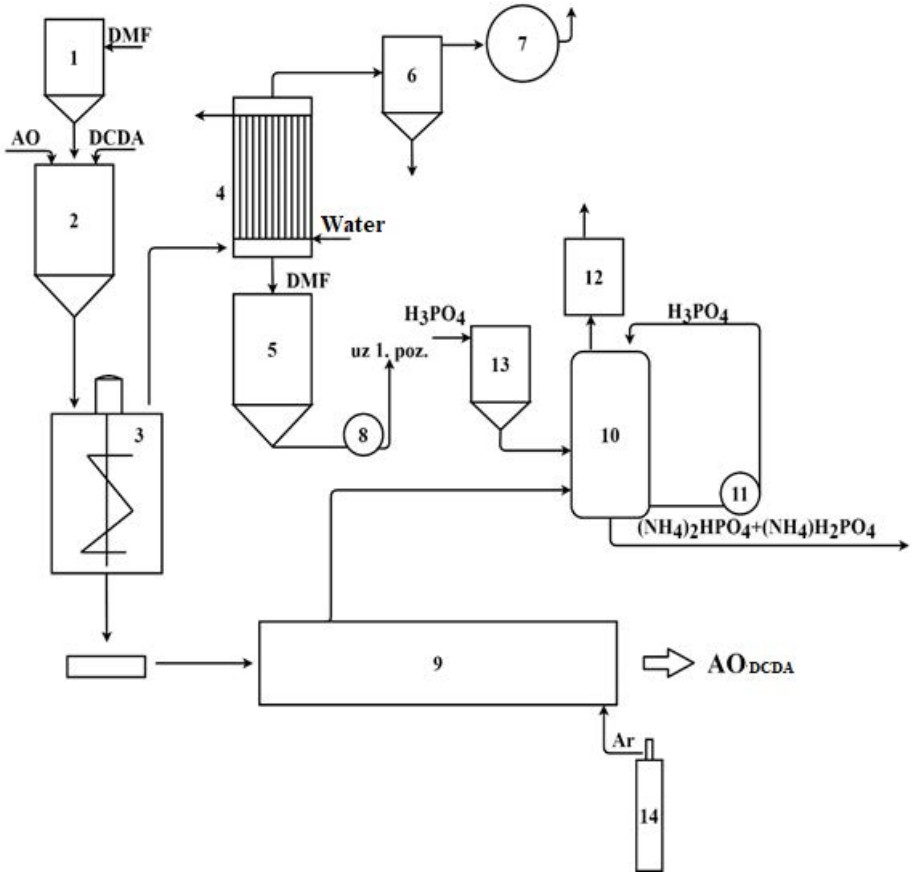

Fig. 18. Technological scheme of AO $_{DCDA}$ production.

The total balance of raw materials and energy resources per 1 t of AO $_{DCDA}$ is given in Table 9.

Table 9

Total Balance of Raw Materials and Energy Resources per 1 t AO $_{DCDA}$

No.	Raw material	Units	Specific consumption per 1 ton of AC (a.d.)
1	Activated carbon	kg	1060
2	DCDA	kg	20 400
3	DMF	kg	110
4	Argon 4.0	m^3	560
5	Electric power	kWh	32 428

CONCLUSIONS

1. The principal possibility has ben researched and the basics of technology for obtaining doped micro-, mesoporous carbon materials using various types of carbonisation and subsequent chemical activation with NaOH, from wood, its processing residues and wood char have been developed.

2. The influence of carbonisation, activation and doping regimes and reagents on the porous structure of the material, the properties of the obtained carbon materials and the possible use in fuel cells as a catalyst for oxygen reduction have been evaluated.

3. It has been proved that under constant activation conditions the pore distribution changes depending on the raw material, carbonisation environment and process parameters (temperature, time). As a result of hydrothermal carbonisation of wood, compared to thermal carbonisation in an inert gas environment, the material has a less dense morphology and 7 times larger average pore width than pyrolysis carbonate.

4. It has been established that more nitrogen can be introduced into disordered carbon material structures that contain more oxygen. It has been proven, that doping with melamine, it binds to the outer wall of the activated carbon pores and, as a result of the polymerization of the reagent, clogs part of the pores, while dicyandiamide binds to the surfaces of the pore walls, practically without changing the pore volume.

5. It is estimated that the nitrogen content of various raw materials AO (T_{akt} = 700, K = 3) after doping is about 5 %. Of these, the most active pyridine in the N form is about 39 % for wood char-based catalysts, the rest is 50 %, regardless of the doping reagent. Reheating of doped activated carbon based on wood char at 800 °C reduces the nitrogen content but increases the pyridine N form content to 59 %, thus increasing the activity of the catalyst and increasing the number of transferred electrons in the fuel cells.

6. It has been shown that by using the obtained carbon material (which has not undergone repeated heat treatment) in the fuel cells, the number of transferred electrons increases with the increase of the ratio of meso- and micro-pores. The most efficient electron transfer occurs when the mesopore volume of a material is larger than the micropore volume, at a constant total pore volume.

7. It has been determined that by using three-stage thermochemical process (carbonisation, activation, and doping with dicyandiamide), it is possible to obtain oxygen reduction reaction activated carbon catalysts based on hydrothermally carbonisated wood carbonisate, black liquor, and wood char (with and without reheating) with properties competitive to a commercial 20 % Pt / C catalyst.

8. Based on the experimental results obtained in the work, a technological scheme for the production of nanoporous AO $_{DCDA}$ from AO, which is obtained from conventional wood char, has been developed. The total and main material and energy consumption of AO DCDA production stages for 1 t AO $_{DCDA}$ production is calculated.

REFERENCES

[1] "Priorities for critical materials for a circular economy," EASAC policy report 29, 2016.

[2] T. Khadiran, M. Z. Hussein, Z. Zainal, and R. Rusli, "Activated carbon derived from peat soil as a framework for the preparation of shape-stabilized phase change material," *Energy*, vol. 82, pp. 468–478, Mar. 2015.

[3] A. Voļperts, *Multifunkcionālie Oglekļa materiāli uz lignoceluložu bāzes*. Rīga, 2017.

[4] X. Z. Yuan and H. Wang, "PEM fuel cell fundamentals," in *PEM Fuel Cell Electrocatalysts and Catalyst Layers: Fundamentals and Applications*, Springer London, 2008, pp. 1–87.

[5] L. Khotseng, "Oxygen Reduction Reaction," in *Electrocatalysts for Fuel Cells and Hydrogen Evolution – Theory to Design*, IntechOpen, 2018.

[6] H. S. Kambo and A. Dutta, "A comparative review of biochar and hydrochar in terms of production, physico-chemical properties and applications," *Renew. Sustain. Energy Rev.*, vol. 45, pp. 359–378, May 2015.

[7] J. Lee, K. H. Kim, and E. E. Kwon, "Biochar as a Catalyst," *Renewable and Sustainable Energy Reviews*, vol. 77. Elsevier Ltd, pp. 70–79, 01-Jan-2017.

[8] G. Dobele, A. Volperts, L. Jašina, and A. Žūrinš, "Synthesis and research of carbon materials with controlled porosity," in *Nanostructured Composite Materials for Energy Storage and Conversion: collection of articles*, Riga: Latvijas Universitātes Akadēmiskais apgāds, 2019, pp. 9–24.

[9] X. Cao, S. Sun, and R. Sun, "Application of biochar-based catalysts in biomass upgrading: A review," *RSC Advances*, vol. 7, no. 77. Royal Society of Chemistry, pp. 48793–48805, 16-Oct-2017.

[10] F. Cheng and X. Li, "Preparation and Application of Biochar-Based Catalysts for Biofuel Production," *Catalysts*, vol. 8, no. 9, p. 346, Aug. 2018.

[11] A. Plavniece, A. Zhurinsh, G. Dobele, and J. Locs, "Chemically Activated Hydrochar Flakes from Birch Wood," *Key Eng. Mater.*, vol. 800, no. 1, pp. 261–266, Apr. 2019.

[12] G. Dobele, E. Jakab, A. Volperts, Z. Sebestyén, A. Zhurins, and G. Telysheva, "Formation of nanoporous carbon materials in conditions of thermocatalytic synthesis," *J. Anal. Appl. Pyrolysis*, vol. 103, pp. 173–180, Sep. 2013.

[13] J. C. C. Freitas, M. A. Schettino, F. G. Emmerich, A. Wong, and M. E. Smith, "A multiple-field 23Na NMR study of sodium species in porous carbons," *Solid State Nucl. Magn. Reson.*, vol. 32, no. 4, pp. 109–117, Dec. 2007.

[14] H. Marsh, D. S. Yan, T. M. O'Grady, and A. Wennerberg, "Formation of active carbons from cokes using potassium hydroxide," *Carbon N. Y.*, vol. 22, no. 6, pp. 603–611, 1984.

[15] R. C. Bansal and M. Goyal, *Activated Carbon Adsorption*, 1st Editio. CRC Press, 2005.

[16] F. Rouquerol, J. Rouquerol, K. S. W. Sing, P. Llewellyn, and G. Maurin, *Adsorption by powders and porous solids*. Academic Press, 2014.

[17] S. Wang, Z. Cui, J. Qin, and M. Cao, "Thermally removable in-situ formed ZnO template for synthesis of hierarchically porous N-doped carbon nanofibers for enhanced electrocatalysis," *Nano Res.*, vol. 9, no. 8, pp. 2270–2283, Aug. 2016.

[18] W. He, C. Jiang, J. Wang, and L. Lu, "High-rate oxygen electroreduction over graphitic-N species exposed on 3D hierarchically porous nitrogen-doped carbons," *Angew. Chemie – Int. Ed.*, vol. 53, no. 36, pp. 9503–9507, Sep. 2014.

[19] R. Wu *et al.*, "Controlled synthesis of hollow micro/meso-pore nitrogen-doped carbon with tunable wall thickness and specific surface area as efficient electrocatalysts for oxygen reduction reaction," *J. Mater. Chem. A*, vol. 4, no. 7, pp. 2433–2437, Feb. 2016.

[20] S. Li, C. Cheng, H.-W. Liang, X. Feng, and A. Thomas, "2D Porous Carbons prepared from Layered Organic-Inorganic Hybrids and their Use as Oxygen-Reduction

Electrocatalysts," *Adv. Mater.*, vol. 29, no. 28, p. 1700707, Jul. 2017.
[21] C. Du *et al.*, "Balancing the Micro-Mesoporosity for Activity Maximization of N-Doped Carbonaceous Electrocatalysts for the Oxygen Reduction Reaction," *ChemSusChem*, vol. 12, no. 5, pp. 1017–1025, Mar. 2019.
[22] J. C. Li *et al.*, "A 3D bi-functional porous N-doped carbon microtube sponge electrocatalyst for oxygen reduction and oxygen evolution reactions," *Energy Environ. Sci.*, vol. 9, no. 10, pp. 3079–3084, Oct. 2016.
[23] M. Seredych, D. Hulicova-Jurcakova, G. Q. Lu, and T. J. Bandosz, "Surface functional groups of carbons and the effects of their chemical character, density and accessibility to ions on electrochemical performance," *Carbon N. Y.*, vol. 46, no. 11, pp. 1475–1488, Sep. 2008.
[24] H. S. Oh, J. G. Oh, W. H. Lee, H. J. Kim, and H. Kim, "The influence of the structural properties of carbon on the oxygen reduction reaction of nitrogen modified carbon based catalysts," *Int. J. Hydrogen Energy*, vol. 36, no. 14, pp. 8181–8186, Jul. 2011.
[25] C. V. Rao, C. R. Cabrera, and Y. Ishikawa, "In search of the active site in nitrogen-doped carbon nanotube electrodes for the oxygen reduction reaction," *J. Phys. Chem. Lett.*, vol. 1, no. 18, pp. 2622–2627, Sep. 2010.
[26] L. Lai *et al.*, "Exploration of the active center structure of nitrogen-doped graphene-based catalysts for oxygen reduction reaction," *Energy Environ. Sci.*, vol. 5, no. 7, pp. 7936–7942, Jul. 2012.
[27] E. J. Biddinger and U. S. Ozkan, "Role of graphitic edge plane exposure in carbon nanostructures for oxygen reduction reaction," *J. Phys. Chem. C*, vol. 114, no. 36, pp. 15306–15314, Sep. 2010.
[28] Y. She *et al.*, "Oxygen Reduction Reaction Mechanism of Nitrogen-Doped Graphene Derived from Ionic Liquid," in *Energy Procedia*, 2017, vol. 142, pp. 1319–1326.
[29] J. D. Wiggins-Camacho and K. J. Stevenson, "Effect of Nitrogen Concentration on Capacitance, Density of States, Electronic Conductivity, and Morphology of N-Doped Carbon Nanotube Electrodes," *J. Phys. Chem. C*, vol. 113, no. 44, pp. 19082–19090, Nov. 2009.
[30] D. Guo, R. Shibuya, C. Akiba, S. Saji, T. Kondo, and J. Nakamura, "Active sites of nitrogen-doped carbon materials for oxygen reduction reaction clarified using model catalysts," *Science (80-.).*, vol. 351, no. 6271, pp. 361–365, Jan. 2016.
[31] K. Derelizade, F. Venturi, R. G. Wellman, A. Khlobystov, and T. Hussain, "Structural changes of thermal sprayed graphene nano platelets film into amorphous carbon under sliding wear," *Appl. Surf. Sci.*, vol. 528, Oct. 2020.
[32] A. Ambrosi *et al.*, "Graphene and its electrochemistry-an update," *Chemical Society Reviews*, vol. 45, no. 9. Royal Society of Chemistry, pp. 2458–2493, 07-May-2016.
[33] K. Kaare *et al.*, "Highly active wood-derived nitrogen-doped carbon catalyst for the oxygen reduction reaction," *ACS Omega*, vol. 5, no. 37, pp. 23578–23587, Sep. 2020.